Renewable and Sustainable Energy Reviews 37 (2014) 47–68

Contents lists available at ScienceDirect

Renewable and Sustainable Energy Reviews

journal homepage: www.elsevier.com/locate/rser

A review of imidazolium ionic liquids research and development towards working pair of absorption cycle

Danxing Zheng *, Li Dong, Weijia Huang, Xianghong Wu, Nan Nie

College of Chemical Engineering, Beijing University of Chemical Technology, Beijing, China

ARTICLE INFO

Article history:
Received 16 December 2013
Received in revised form
8 April 2014
Accepted 12 April 2014
Available online 26 May 2014

Keywords:
Ionic liquid
Working pair
Absorption cycle
Thermophysical property

ABSTRACT

The concerns of energy consumption and environment pollution urge researchers to work on the development of clean energy and the utilization of waste energy. As one important topic, absorption cycle technology has attracted considerable attention because it can be powered by low-grade heat, e.g., solar energy and waste heat. In recent years, researchers proposed that ionic liquids (ILs) as novel alternative absorbent combined with refrigerant such as water, ammonia, alcohols, and hydrofluorocarbons can be used as working pairs for absorption refrigeration cycle, heat pump, and absorption power cycle. In this paper, researches done in imidazolium IL working pairs regarding to status of evaluation and selection methods, thermophysical property measurement and modeling, as well as their future prospect assessments, i.e., developing potential studies about the absorption cycle performance adopting new working pairs, have been reviewed.

Contents

* Correspondence to: P.O. Box 100, College of Chemical Engineering, Beijing University of Chemical Technology, Beijing 100029, China. Tel./fax: +86 10 6441 6406.
E-mail address: dxzh@mail.buct.edu.cn (D. Zheng).

http://dx.doi.org/10.1016/j.rser.2014.04.046
1364-0321/

1. Introduction

1.1. Significance of R&D of absorption cycle and ionic liquid working pair

To deal with the changes in global climate, rapid growth of energy demand and rapid development of renewable energy and energy utilization, much attention has been focused on the research and development (R&D) of absorption cycles, such as absorption heat pump and absorption refrigeration cycle, because they can make effective use of low-grade heat [1–4]. However, the R&D of absorption technology faces a series of problems. For example, the temperature range of the heat source is wider, with a range of 80 – 90 °C collected by economic and efficient flat solar collectors to 500 – 600 °C exhausted from gas turbines or internal combustion engines. The functions and configurations of new absorption cycles are more diverse and complex, such as cogeneration systems that combine power and refrigeration cycles [5–7], compression and absorption hybrid cycles driven by low-grade heat and electrical energy [8,9], and distributed energy systems that combine cooling, heating, and power cycles [10] involving energy storage [11–15] and absorption technologies [16–18]. The above developments present new demands for the R&D of working pairs of absorption cycles as a key and essential work.

Generally, the working pair of absorption cycle is a multi-species solution, which is usually a binary solution consisting of two species with a large boiling point difference. The species with relatively low boiling point, i.e., the volatile species, acts as refrigerant, whereas the species with high boiling point, i.e., the non-volatile species, acts as absorbent. The main types, existing problems, and requests for future development of the absorption cycle working pairs are briefly summarized and listed in Table 1. Based on the species of refrigerant, the working pairs are divided into the following five categories: water, ammonia, alcohol, halohydrocarbon and hydrocarbon (HC). The combinations of five kinds of refrigerants and different absorbents can basically meet the needs of different applications. For example, the H_2O/LiBr working pair is mainly applied in room air conditioning. The NH_3/H_2O working pair can meet cooling requirements below 0 °C. The two working pairs described above are the most widely used systems with environmentally friendly features.

However, the H_2O/LiBr system presents certain disadvantages, such as crystallization, corrosion, and negative pressure operation. Some researchers have attempted to improve the H_2O/LiBr working pair by adding auxiliary species [19,20]. The NH_3/H_2O system also has some drawbacks, such as difficulty in separation and toxicity. Some researchers have added non-volatile species to reduce the separation difficulty [21–23].

Alcohol working pairs are mainly composed of low carbon alcohols, such as methanol and ethanol, or fluoroalcohols, such as 2,2,2-trifluoroethanol (TFE) and hexafluoroisopropanol (HFIP), as refrigerant and salts or high-boiling point organics as absorbent. Alcohols are inflammable and methanol is toxic, so greater interest has been given to fluoroalcohols. Fluoroalcohols are non-corrosive, non-combustible, and have good thermal characteristics. TFE composed of working pairs with some high-boiling point organics have been used, such as tetraethylene glycol dimethyl ether (E181) [24,25], N-methyl-2-pyrrolidone (NMP) [26], N,N′-dimethylpropyleneura (DMPU) [27], N,N′-dimethylethyleneurea (DMEU) [27], and quinoline [28,29]. These working pairs generally have no crystal restrictions, and therefore, have relatively wide operating ranges.

Hydrofluorocarbons (HFCs) are refrigerants with benign technical properties, which are extensively used in the vapor compression refrigeration cycle. It is worth mentioning that HFCs used in the absorption refrigeration cycle are almost harmless to the atmospheric ozone, whereas chlorofluorocarbons (CFCs) are harmful to the atmospheric ozone commonly cannot be used for the absorption refrigeration cycle [30]. HC working pairs have also attracted widespread attentions because of their naturally eco-friendly feature [8,31]. However, due to the flammability and explosibility, researches and applications of HC working pairs are impeded by numerous restrictions.

Both H_2O/LiBr and NH_3/H_2O systems can be developed for future applications, but existing problems need to be solved urgently. Unlike H_2O and NH_3, absorbents suitable for alcohols, HFCs, and HCs are still quite few. Considering that HFCs and HCs can meet the refrigeration technology demands of H_2O and NH_3, absorption cycle working pairs containing HFC or HC have great potential for exploration and are expected to fill the gaps of H_2O/LiBr or NH_3/H_2O systems. Around exploring advanced absorbents with HFC and HC, researchers are exerting efforts to develop novel absorption cycle working pairs [27,32].

Table 1
R&D of absorption cycle working pairs.

Refrigerant species	Absorbent species	Existing problems	Main of the past R&D	Requests of future development
H_2O	LiBr	Corrosion, crystallization	Adding other auxiliary species, e.g., octanol and other species	Abate or avoid the problems of corrosion and crystallization
NH_3	H_2O	Toxicity, difficulty in separating NH_3 from H_2O	Other organic ammoniates	Reduce the separating energy consumption
HFC & HC	Organic solvents	1) Absences of techno-economic significance 2) Values of ODP[a] and GWP[b] cannot meet the needs of developing	New refrigerants with higher ODP and GWP values	1) Meet needs of the R&D of new refrigerants, e.g., R152a, R32 2) Suitable for novel hybrid cycles and co-generation cycles
Alcohol (CH_3OH, C_2H_5OH, TFE)	Organic solvents	To be devoid of techno-economic significance as like as the system H_2O/LiBr	Few	Better techno-economic significance, and environmentally friendly characteristics

[a] Ozone depletion potential.
[b] Global warming potential.

1.2. Basic properties and characteristics of ILs used as absorbent species

ILs are composed of ions, and generally consist of organic cations containing nitrogen or phosphorus and organic or inorganic anions [33]. In 1992, Wilkes et al. [34] published reports on synthesis and performance of 1-ethyl-3-methylimidazolium tetrafluoroborate ($[EMIM]BF_4$). They found that this IL is moisture stable, does not undergo hydrolysis, has a low melting point, and has good thermal stability. Thereafter, the study of ILs has been greatly promoted, constantly developed, and emerged worldwide upsurge.

Variety species of ILs exist, and their physicochemical properties can be regulated by changing the type and structure of anions and cations. Thus, ILs are called designable solvents [35,36]. Generally, based on the types of organic cation, ILs can be divided into imidazolium, pyridinium, tetraalkyl ammonium, tetraalkyl phosphonium, and so on [37,38]. Common cationic structures are shown in Fig. 1. Among ILs mentioned above, imidazolium ILs are the most stable, most common, and most studied.

According to the solubility differences of ILs and water, ILs can be divided into two categories: hydrophilic ILs, such as 1-alkyl-3-methylimidazolium chloride ($[C_nMIM]Cl$, n is the number of C atom in the alkyl, $n=1, 2, 3,\ldots$), 1-alkyl-3-methylimidazolium tetrafluoroborate ($[C_nMIM]BF_4$), 1-alkyl-3-methylimidazolium dimethylphosphate ($[C_nMIM]DMP$), 1-alkyl-3-methylimidazolium methylsulfate ($[C_nMIM]MeSO_4$), and 1-alkyl-3-methylimidazolium ethylsulfate ($[C_nMIM]EtSO_4$), and hydrophobic ILs, such as 1-alkyl-3-methylimidazolium hexafluorophosphate ($[C_nMIM]PF_6$), 1-alkyl-3-methylimidazolium trifluoromethanesulfonate ($[C_nMIM]TfO$), and 1-alkyl-3-methylimidazolium bis(trifluoromethylsulfonyl)imide ($[C_nMIM]Tf_2N$) [39,40]. The hydrophilicity and hydrophobicity of ILs are affected by type and structure of anions and cations. Usually, a shorter alkyl side chain leads to stronger hydrophilicity of IL, conversely, a longer alkyl side chain leads to stronger hydrophobicity of IL.

As a new kind of environmentally friendly solvents, ILs have been widely utilized in chemical reactions, catalysis, separation, and electrochemistry [36,40,41]. Moreover, ILs can be used as absorbent species in combination with refrigerants to constitute new working pairs for absorption cycle. Compared with organic solvents, the advantages of IL are mainly embodied in the following aspects.

(1) Most ILs exist as liquid at a wide range around room temperature. The boiling points of ILs are much higher than those of refrigerants because of the ignorable vapor pressure. In the generation process, the refrigerant can be easily separated from IL with high purity in the cycle.
(2) The heat capacity of IL solution is small, which is beneficial in improving the cycle efficiency.
(3) Solubilities with inorganic or organic species and the affinity with refrigerants are good, which is in favor of enhancing the mass transfer.
(4) ILs have high chemical and thermal stability, high thermal decomposition temperature, and are non-flammable.
(5) The chemical and physical properties of ILs can be adjusted by the design of anion and cation.

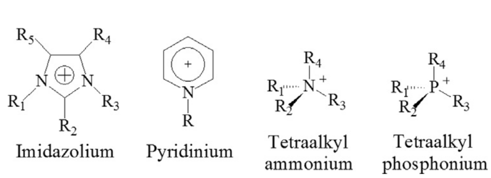


Fig. 1. Structure of the cations of the common ILs.

Many research groups have investigated the thermophysical properties of working pairs consisting of ILs and common refrigerants, such as H_2O, NH_3, alcohol, and HFCs, for absorption cycle [42–45]. These researches exhibit the great potential and significant application prospects of these novel working pairs.

1.3. Previous studies

In 2004, Kim et al. [42] proposed some working pairs composed of imidazolium ILs (1-butyl-3-methylimidazolium tetrafluoroborate ($[BMIM]BF_4$), 1-butyl-3-methylimidazolium bromide ([BMIM]Br)) and refrigerants (TFE, 1,1,1,2-tetrafluoroethane (R134a)). Among these systems, TFE/[BMIM]Br and TFE/$[BMIM]BF_4$ were selected as alternative working pairs for absorption refrigeration cycle and heat pumps. The investigated results of heat capacity and vapor pressure of the two systems show that [BMIM]Br and TFE had a stronger interaction, and IL working pairs generally have good thermodynamic properties and deserve further study.

Since 2006, Shiflett and Yokozeki [46–48] from DuPont Company have published lots of patents and papers on the use of ILs as absorbents, which are impressive researches at this field in recent decade. The solubilities and diffusivities of H_2O [49], NH_3 [23,50], CO_2 [44,51] and HFCs [52–62] in ILs were measured, and some new working pairs for absorption cycle were proposed, such as $H_2O/[EMIM]BF_4$, NH_3/[DMEA]Ac (N,N-dimethylethanolammonium acetate), and R134a/[EMIM]BEI (1-ethyl-3-methylimidazolium bis (pentafluoroethylsulfonyl)imide).

In 2006, Sen and Paolucci [45] presented that IL 1-butyl-3-methylimidazolium hexafluorophosphate ($[BMIM]PF_6$) can be used in absorption refrigeration cycle with CO_2. Some properties, such as vapor pressure, thermal stability, and dissolve ability, were discussed, which demonstrated that thermodynamic data of IL working pair systems are still lacking. In 2010, Martín et al. [63] selected appropriate IL and supercritical CO_2 as working pairs and calculated the coefficient of performance (*COP*) for absorption refrigeration cycle based on the phase equilibrium of the system. However, because of the necessity of operating with a higher circulation ratio, the *COP* was lower than that of the conventional system NH_3/H_2O. In 2012, Kim et al. [64,65] conducted theoretical researches about the thermodynamic performance of a miniature absorption refrigeration system with refrigerant/IL as working pairs. Previously studied ILs including 1-ethyl-3-methylimidazolium bis(trifluoromethylsulfonyl)imide ($[EMIM]Tf_2N$), $[EMIM]BF_4$, $[BMIM]BF_4$, $[BMIM]PF_6$, 1-hexyl-3-methylimidazolium bis(trifluoromethylsulfonyl)imide ($[HMIM]Tf_2N$), 1-hexyl-3-methylimidazolium tetrafluoroborate ($[HMIM]BF_4$), and 1-hexyl-3-methylimidazolium hexafluorophosphate ($[HMIM]PF_6$), as well as refrigerants including H_2O, pentafluoroethane (R125), R134a, 1,1,1-trifluoroethane (R143a), 1,1-difluoroethane (R152a), difluoromethane (R32), 1,2-dichloro-1,1,2,2-tetrafluoroethane (R114), and 1,1,2,2-tetrafluoroethane (R134). *COP* and feasibility were calculated and compared. Results showed that among these systems, $H_2O/[EMIM]BF_4$ had the highest *COP* with a value of 0.91.

Liang et al. [66] and Zhao et al. [67] determined the heat capacity, viscosity, density and phase equilibrium for methanol/[BMIM]Cl (1-butyl-3-methylimidazolium chloride) and methanol/[DMIM]DMP (1,3-dimethylimidazolium dimethylphosphate) systems. They also analyzed the potential of the two systems, which were found to meet the requirements of benign working pairs of absorption cycle.

In 2011, Zhang et al. [68] evaluated the performance of the H_2O/[EMIM]DMP (1-ethyl-3-methylimidazolium dimethylphosphate) system in absorption refrigeration cycle, results indicated that its

COP was lower than that of the traditional H_2O/LiBr system but still higher than 0.7. Moreover, the generation temperature of the H_2O/[EMIM]DMP system was lower than that of the H_2O/LiBr system, showing that the new cycle could be driven by waste heat or hot water with lower temperature. Zhang et al. [69,70] also simulated the thermodynamic performance of the heat pump using H_2O/[EMIM]DMP and H_2O/[DMIM]DMP systems as working pairs, and compared the result with that of H_2O/LiBr and TFE/E181 systems. The results indicated that the *COP* of H_2O/[EMIM]DMP and H_2O/[DMIM]DMP systems were slightly lower than that of the H_2O/LiBr system, but significantly higher than the value of the TFE/E181 system.

Since 2007, author's group has conducted numerous theoretical and experimental studies on IL working pairs, and published several related papers [71–83]. Based on the solution thermodynamic theory, the excess Gibbs function (G^E) evaluation method is expanded to IL working pairs using the UNIFAC model as calculation tool, and this method is applied in the screening of H_2O/IL, NH_3/IL, and HFC/IL systems. According to the evaluation method, hydrophilic IL 1,3-dimethylimidazolium chloride ([DMIM]Cl) was selected and synthesized. A variety of experimental methods were adopted to determine thermophysical properties, such as density, heat capacity, vapor pressure and solubility, for H_2O/IL, NH_3/IL, and HFC/IL systems. Appropriate thermodynamic models were chosen to regress and predict the properties of selected systems. The influence of ILs as additives in traditional H_2O/LiBr and NH_3/H_2O systems was investigated. Furthermore, the characteristics of absorption refrigeration cycle and heat pump using IL working pairs were simulated and calculated.

Refrigerant/IL systems have increasingly received much attention as novel, environmentally friendly working pairs. Researches show that IL working pairs can extend the operating temperature range of the cycle and strengthen the separation and generation processes of absorbate, thus reducing the energy consumption and potentially reducing or eliminating corrosion and crystallization. Proper combinations of refrigerant and IL may generate new working pairs with excellent performance. However, some problems with IL working pairs are still encountered, such as high circulation ratio and low energy conversion efficiency, showing the necessity for further development. Fortunately, ILs have huge species number, and their functions can be designed by changing the structure of cation and the species of anion to meet the increasing demands for new working pairs. Therefore, selecting more valuable working pairs from a large number of research objects, measuring necessary chemical and physical properties of new systems with high accuracy, establishing corresponding models of physical and chemical properties, and evaluating the application significances of new IL working pairs, are still challenging issues that must be overcome to accelerate the application progress of IL working pairs.

1.4. Focus and proposals of this work

This work aims to exhibit the international research frontier of absorption cycle IL working pairs in recent years to make relevant researches more rational and efficient. The evaluation method for IL working pairs was introduced, which was based on macroscopic properties and intermolecular interactions, combining the UNIFAC model with extreme G^E criterion. The research progress on the thermophysical properties of IL working pairs was presented, including the measurement method and modeling of vapor pressure, solubility, heat capacity and density for popular systems. Particularly, on the basis of researches on thermophysical properties of systems containing refrigerants H_2O, NH_3, and HFCs, several binary and ternary systems with potential have been presented. Finally, the performance of absorption cycle using IL working pairs was calculated and evaluated to verify further the future developmental potential of new systems.

2. Selection of IL absorbent for working pair innovation

2.1. General behaviors of the vapor–liquid equilibrium

The activity coefficient of the refrigerant in IL can be calculated using the vapor–liquid equilibrium (VLE) data of IL working pairs and can be used to quantitatively characterize the volatility of refrigerant and the solubility in IL, establish the thermodynamic model of IL working pair, analyze the influence of component structure on the interaction between refrigerant and IL, and guide the selection and optimization of IL absorbent.

For refrigerant (1)/IL (2) binary systems, the concentration of IL in the gas phase can be neglected, i.e., the gas phase mole fraction of the refrigerant species is equal to 1. Hence, the VLE relationship can be expressed as [84]

$$p(T)=x_1\gamma_1 p_1^s(T) \tag{1}$$

where p is the system pressure, x_1, γ_1, and p_1^s are the liquid phase mole fraction, activity coefficient, and saturated vapor pressure of the refrigerant species, respectively. Generally, the activity coefficient model, Wilson model, UNIQUAC model, NRTL model, and so on can be adopted to correlate the γ_1 based on the experimental VLE data of working pairs. Appropriate model is selected by considering several aspects of theoretical analysis and experimental measurement. Therefore, the activity coefficient value of the refrigerant species γ_1 can be correlated and predicted, while the activity coefficient value of the IL species γ_2 cannot be calculated directly, because ILs have negligible vapor pressure. However, when γ_1 can be estimated, γ_2 can be determined by integration of the Gibbs–Duhem equation at constant temperature and pressure [85].

$$x_1\,\partial \ln\gamma_1/\partial x_2+x_2\,\partial \ln\gamma_2/\partial x_2=0 \tag{2}$$

where x_2 is the liquid phase mole fraction of the IL species. For instance, the activity coefficient of refrigerant species can be represented by an appropriate model [85]

$$\ln\gamma_1=ax_2^2+bx_2^3+cx_2^4 \tag{3}$$

where a, b, and c are concentration-independent parameters. The value of $\ln\gamma_2$ for the IL species can then be obtained in terms of the same parameters.

In addition, the partial pressure of Raoult's law used for describing the VLE behavior of the refrigerant in a liquid ideal mixture is expressed as [84]

$$p_1^{RL}(T)=x_1 p_1^s(T) \quad (i=1,2,\ldots,N) \tag{4}$$

In a $p-x(y)$ diagram, Eq. (4) exhibits a straight line. The $p-x(y)$ curve of the non-ideal mixtures that display positive deviation from Raoult's law falls above the line; whereas the $p-x(y)$ curve of the non-ideal mixtures that show negative deviation from Raoult's law falls below the line, causing the negative deviation of the liquid phase from the ideal mixtures, exhibiting the value of γ_i is less than 1.

In the view of vapor pressure criterion for selecting absorption cycle working pairs, systems with strong absorbing ability are usually classified as exhibiting negative deviation from Raoult's law [86]. Working pairs exhibiting highly negative deviation from Raoult's law produce the best results, as Morrissey has described [87]. The solvent vapor pressure decreases because the solvent molecules in the liquid phase have strong affinity to the solute molecules.

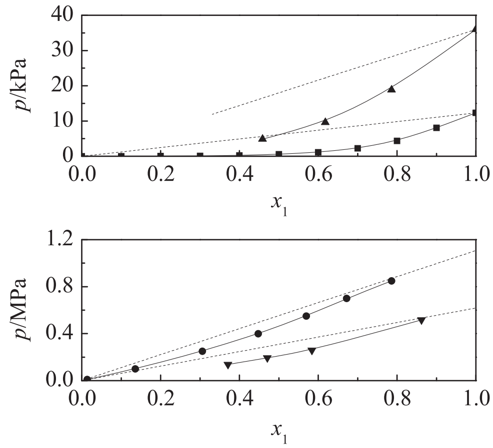


Fig. 2. Vapor pressure-composition diagram of several IL working pairs. ■, H_2O/[DMIM]DMP, 323.2 K [72]; ▲, TFE/[EMIM]BF_4, 323.15 K [80]; ●, R32/[EMIM]Tf_2N, 283.15 K [54]; ▼, NH_3/[BMIM]PF_6, 283.4 K [23]. Dashed line: Raoult's law.

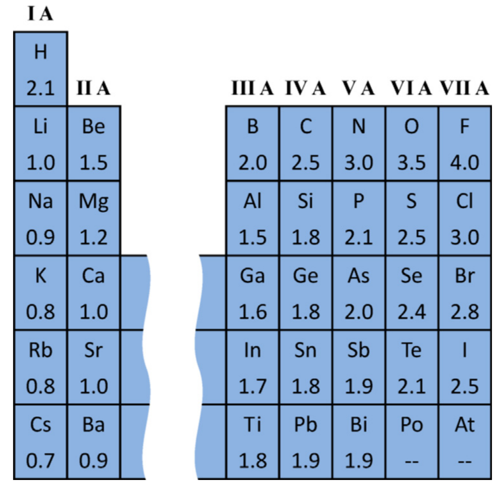


Fig. 3. Some atoms electronegativity values (Pauling scale).

Table 2
Bond energy and bond length of some hydrogen bonds [86].

Hydrogen bond	Bond energy/kJ mol^{-1}	Bond length/pm	Compounds
F—H····F	28.1	255	$(HF)_n$
O—H····O	18.8	276	H_2O (ice)
O—H····O	25.9	266	CH_3OH, C_2H_5OH
N—H····F	20.9	268	NH_4F
N—H····O	20.9	286	CH_3CONH_2
N—H····N	5.4	338	NH_3

Studies on available IL working pairs of binary and ternary systems and common refrigerants H_2O, NH_3, alcohols, HCs, and HFCs have shown that the VLE behaviors of IL working pairs generally manifest as non-ideal mixtures. For example, the vapor pressure-composition ($p-x$) diagram in Fig. 2 describes the behavior of several IL working pairs showing negative deviation from Raoult's Law.

2.2. Effects of the molecular structure

Essentially, the non-ideal VLE behavior of the working pair depends on intermolecular force, which includes the interaction between different molecules and homologous molecules for a multi-species system. The quantitative relationships for contacting intermolecular forces and macroscopic properties are now confined to simple idealized systems. The mechanism underlying solubility difference among IL working pairs is not clear at the molecular level, the hydrogen bond is only known to play an important role [62,88].

The hydrogen bond can be simply expressed as X—H····Y, where the dotted line represents the hydrogen bond. Based on the formation theory of hydrogen bond, the strength of the hydrogen bond is associated with the electronegativity of X and Y atoms connected with the H atom. The stronger the electronegativity of X and Y atoms is, the stronger the hydrogen bond will be. Meanwhile, the hydrogen bond is also influenced by the radius of the Y atom. A smaller the radius of the Y atom results in a stronger hydrogen bond. The bond energy and bond length of some hydrogen bonds are listed in Table 2 [89]. Some atomic electronegativity values (Pauling scale) are shown in Fig. 3 [90]. In the H_2O molecule, the electronegativity of the O atomic is larger, so that the H atom has excess force to form a hydrogen bond with highly electronegative atom in other molecules, such as F, O and N. Fig. 4(a) schematically shows the hydrogen bond between hydrophilic IL and H_2O. As shown in [DMIM]Cl aqueous solution, the H atom in H_2O molecule and the Cl atom in IL anion of form hydrogen bond O—H····Cl. Fig. 4(b) shows the hydrogen bonding interaction between R32 and [BMIM]Tf_2N (1-butyl-3-methylimidazolium bis(trifluoromethylsulfonyl)imide). The imidazole ring of IL has three hydrogen bond donors (H1, H2, H3), but only two proton acceptors (two F atoms) in the R32 molecule, so two hydrogen bonds are formed. The anion $[Tf_2N]^-$ has 10 proton acceptors (O1, O2, O3, O4, F1, F2, F3, F4, F5, and F6), but the R32 molecule only has two hydrogen donors (two H atoms), so two hydrogen bonds are also formed.

Generally, the electronegativity of the C atomic is small, and C—H is generally difficult to form hydrogen bond. However, the C atom between two N atoms in the imidazole ring of cation will form a hydrogen bond because the electronegativity increases due to the highly electronegative neighboring two N atoms. Therefore, in IL aqueous solution, the O atom in a H_2O molecule can easily form a hydrogen bond with the H atom on the C atom between two N atoms in the imidazole ring, while the interaction with the H atoms on the other two C atoms in the imidazole ring is weak. When the length of alkyl side chain of cation in IL decreases, the volume of cation decreases, the surface charge density increases, and the electrostatic interaction between cation and H_2O molecule enhances. Correspondingly, the ability of IL binding together with H_2O molecule enhances, showing that a shorter cationic alkyl side chain results in better affinity of IL with H_2O. Klimavicius et al. [91] studied hydrogen bond formed in D_2O solutions of 1-decyl-3-methylimidazolium bromide ([C_{10}MIM]Br) and 1-decyl-3-methylimidazolium chloride ([C_{10}MIM]Cl) with ^1H, ^{13}C NMR and Raman spectroscopy monitoring of proton/deuteron process. They found that anions and aggregation effects play crucial role in IL aqueous solutions, anions interact with cations via H-bond and bind water molecules in their solvation shells.

In the study of D'Angelo et al. [92], the interaction of H_2O and Br^- in [BMIM]Br was investigated combining extended X-ray absorption fine structure spectroscopy and molecular dynamics simulations. A picture of structural properties of [BMIM]Br/H_2O was gained, in the surroundings of both the imidazolium cation and anion Br^-. This new approach has been found to be particularly well suited to obtain detailed information on IL solutions despite their complexity.

For the working pairs adopting water as refrigerant, the interaction between water and absorbent needs to be enhanced, so the IL, which has good affinity with water, is studied. The number of ILs is beyond count, because the structure can be designed. The different configurations of the anion and cation

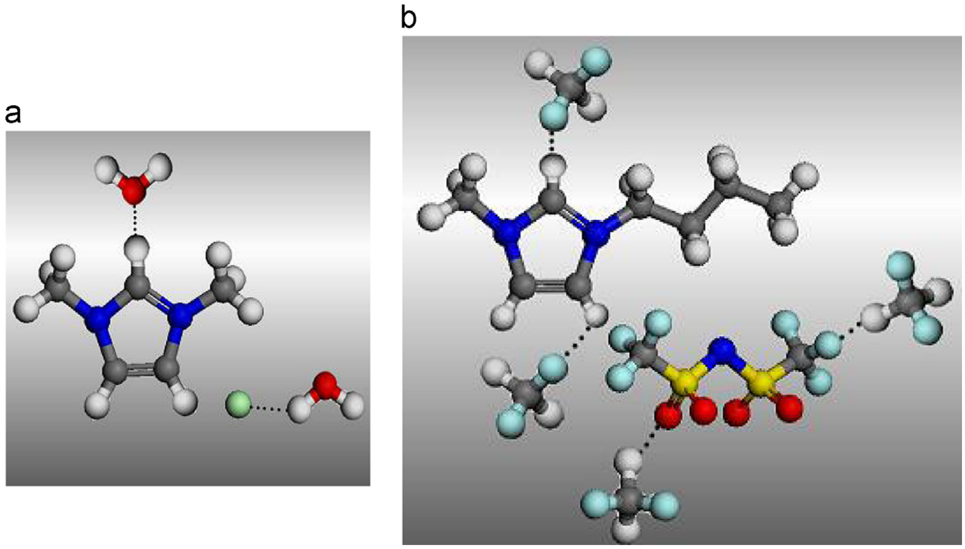


Fig. 4. Hydrogen bonding interaction between refrigerants and ILs. (a) H_2O/[DMIM]Cl and (b) R32/[BMIM]Tf_2N.

Table 3
Relationship of IL anion and water solubility.

Hydrophobic	→	Hydrophilic
PF_6^- $[(CF_3SO_2)_2N]^-$ $[(C_2F_5SO_2)_2N]^-$	BF_4^- $CF_3SO_3^-$	Br^-, Cl^-, I^- CH_3COO^-, $(CH_3)_2PO_4^-$ $CH_3OSO_3^-$, $C_2H_5OSO_3^-$

make ILs show different hydrophilicities. The interaction between IL and water is influenced by the structure, including the organic cationic species, cationic substituent structure, and anionic species. Studies show that for imidazole ILs, increasing of the alkyl side chain of the cation leads to reduce the hydrophilicities of ILs, such as [DMIM]X > [EMIM]X > [BMIM]X > [HMIM]X (X means a certain kind of anion).

The anion characteristics greatly affect the solubility of IL in water. Table 3 lists the relationship between the IL anion and water solubility. Generally, for the solubility of the refrigerant in IL, the anion shows greater effect than the cation [93], because the imidazolium cation only depends on the length of the alkyl side chain or structure to show the impact, while the anion may have greater variety and structural changes.

Similar to H_2O/IL systems, the hydrogen bond has a very important function in HFC/IL systems. The hydrogen bond heavily influences the physical and chemical properties of the IL working pairs. Forming hydrogen bond between solute and solvent will increase the solubility, so IL having good affinity with HFC is sought for HFC/IL working pairs. As in hydrophilicities, the affinity of IL with fluoride is also influenced by the cation species, structure of cation substitution, and anion species. Available experimental results show that for imidazolium ILs, the longer the cationic alkyl side chain is, the better the affinity with HFC will be, as shown in the following rule: [EMIM]X < [BMIM]X < [HMIM]X < [OMIM]X ([OMIM] means 1-octyl-3-methylimidazolium), which is opposite to the hydrophilic of IL [75].

Comparing VLE data of several HFC/IL systems, the effect of anion on the solubility of HFC in IL was as follows: $[C_nMIM]Tf_2N > [C_nMIM]PF_6 > [C_nMIM]TfO \approx [C_nMIM]BF_4$ [75]. The solubility increases with increasing number of fluorine atoms in the anion. The hydrogen bond is only one aspect of the contribution of the IL affinity with fluoride, far from being able to explain the pros and cons on the overall performance of working pairs. Thus, further studies are needed.

2.3. Infinity dilution activity coefficient criterion

The activity coefficient of the refrigerant in working pairs relates to the composition of the system. However, the infinite dilution activity coefficient of the refrigerant (γ_1^∞), calculated on the basis of Henry's law, is a physical quantity that is unrelated to the composition of the system and reflects the regular interaction between refrigerant and IL. At given temperature and pressure, Henry's constant in working pairs is given by

$$k_1 = \lim_{x_1 \to 0} (p/x_1) = \gamma_1^\infty p_1^s(T) \tag{5}$$

where k_1 is Henry's constant. At low vapor pressure of the refrigerant, the solubility of the refrigerant has a linear relationship with vapor pressure, and γ_1^∞ and k_1 can be obtained when the concentration tends to zero, i.e., the slope of the line when pressure tends to zero. In fact, γ_1^∞ and k_1 are direct reflections of the solubility of the refrigerant at low vapor pressure. Smaller values of γ_1^∞ and k_1 mean higher solubility of the refrigerant. Therefore, γ_1^∞ and k_1 can be used to compare the degree of miscibility of the refrigerant and IL.

The absorption potential was proposed as another evaluation criterion for absorption cycle working pairs [83].

$$\psi_1 \equiv 1/\gamma_1^\infty \tag{6}$$

where ψ_1 is the absorption potential. At given temperature and pressure, higher values of ψ_1 result in stronger absorbing ability of the absorbent.

In Table 4, γ_1^∞ decreases with increasing length of cation alkyl side chain. In Table 5, except for 1-butyl-3-methylimidazolium trifluoromethanesulfonate ([BMIM]TfO), γ_1^∞ decreases with increasing number of fluorine atoms of anion. The γ_1^∞ of binary systems composed of nine HFCs, such as R32, R134, with IL [BMIM]PF_6 are listed in Table 6. The HFC containing more carbon atoms and fluorine atoms shows better miscibility with [BMIM]PF_6. In

Table 4
Activity coefficients at infinite dilution of R32 in $[PF_6]$-based ILs at 298.2 K.

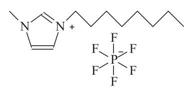
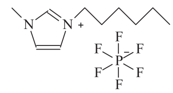
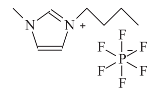
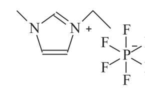
Item	$[OMIM]PF_6$	$[HMIM]PF_6$	$[BMIM]PF_6$	$[EMIM]PF_6$
Absorbent structure				
γ_1^∞	0.4525	0.5559	0.7328	1.1028
ψ_1	2.2099	1.7989	1.3646	0.9068
p_1^s /MPa	1.6919	1.6919	1.6919	1.6919
k_1	0.7656	0.9405	1.2398	1.8658

Table 5
Activity coefficients at infinite dilution of R32 in the [BMIM]-based ILs at 298.2 K.

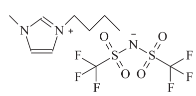
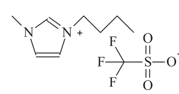
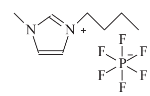
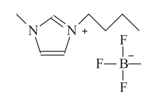
Item	$[BMIM]Tf_2N$	[BMIM]TfO	$[BMIM]PF_6$	$[BMIM]BF_4$
Absorbent structure				
γ_1^∞	0.5026	0.7112	0.7328	0.8794
ψ_1	1.9897	1.4061	1.3646	1.1371
p_1^s /MPa	1.6919	1.6919	1.6919	1.6919
k_1	0.8503	1.2033	1.2398	1.4879

Table 6
Activity coefficients at infinite dilution of various HFCs in the IL $[BMIM]PF_6$ at 298.2 K.

Items	R32	R134	R41	R23	R152a
Refrigerant structure	CH_2F_2	CHF_2CHF_2	CH_3F	CHF_3	CH_3CHF_2
γ_1^∞	0.7328	0.8289	0.8677	1.2847	1.3957
ψ_1	1.3646	1.2064	1.1525	0.7784	0.7165
p_1^s /MPa	1.6919	0.5268	3.8383	4.7044	0.5973
k_1	1.2398	0.4367	3.3305	6.0437	0.8337
Items	**R161**	**R134a**	**R125**	**R143a**	
Refrigerant structure	CH_3CH_2F	CF_3CH_2F	CHF_2CF_3	CH_3CF_3	
γ_1^∞	1.4969	1.8615	3.1726	3.6674	
ψ_1	0.6680	0.5372	0.3152	0.2727	
p_1^s /MPa	0.9230	0.6664	1.3797	1.2632	
k_1	1.3817	1.2404	4.3772	4.6327	

addition, comparing R134 with R134a, γ_1^∞ of R134a is much larger than that of R134 because of isomerization.

2.4. VLE prediction without experimental data by the UNIFAC model

The activity coefficient of the refrigerant species in IL working pairs is the basic data needed for selecting suitable IL absorbents. However, the obtained experimental data are sometimes insufficient. The UNIFAC model provides a calculation method to correlate and predict the activity coefficient without experimental data, which was proposed by Fredenslund based on the group-contribution method in 1975 [94]. The UNIFAC model is specifically suitable for mixtures of molecules, but not for mixtures containing ionic components, because the residual term of the model only considers short-range interactions. To extend the application range of the UNIFAC model, the IL can be considered as a neutral molecule or a weak electrolyte solution. The reasonability of this perspective can be explained from the following aspects [81]. The conductivity of IL is usually very low, at approximately 10^{-3} mS/cm. After dilution in the polar solvent the conductivity will increase by 10–20 times, showing strong association between the anion and the cation, and forming electroneutral ionic clusters [95]. The VLE and LLE data of IL systems can be well described by the G^E model applied for traditional non-electrolyte solutions, such as the NRTL activity coefficient model and PR equation of state (EOS), showing that ILs can be reasonably regarded as molecular components and that the electrostatic interaction can be ignored [54,96]. Using electrospray ionization mass spectrometry, a large amount of ionic clusters in different degrees of association or supramolecular polymerization has been detected in ILs, showing that ILs are similar to neutral molecules or weak electrolytes that can be approximately treated as neutral components.

In the UNIFAC model, the activity coefficient is calculated as a sum of two terms [97],

$$\ln \gamma_i = \ln \gamma_i^C + \ln \gamma_i^R \tag{7}$$

where γ_i is the activity coefficient of component i, γ_i^C is the combinatorial term, and γ_i^R is the residual term. The combinatorial term mainly considers the difference of molecular size and shape. The residual term mainly considers the interaction force between molecules, and can be obtained from the properties of pure substances and mixtures.

To use the UNIFAC model, ILs need to be segmented into groups. ILs can be decomposed through the method presented by Kim [98] and Lei [99]. As shown in Fig. 5, the IL [BMIM]Cl is divided into one CH_3 group, three CH_2 groups, and one [MIM]Cl group. Other ILs can also be divided into groups in the same way.

Based on the study conducted by Lei et al. [99], Dong et al. [71] studied a series of H_2O/IL binary systems, which mainly included three kinds of short carbon chain imidazolium cations, namely, [DMIM], [EMIM] and [BMIM], as well as seven kinds of anions, namely, Cl, Br, BF_4, DMP, DBP (dibutylphosphate), $EtSO_4$, and TfO. Parameters for 14 group pairs were then added to the UNIFAC parameter table. The proposed new group interaction parameters are listed in Table 7, which can be used to predict VLE and excess properties of systems containing H_2O and imidazolium ILs at

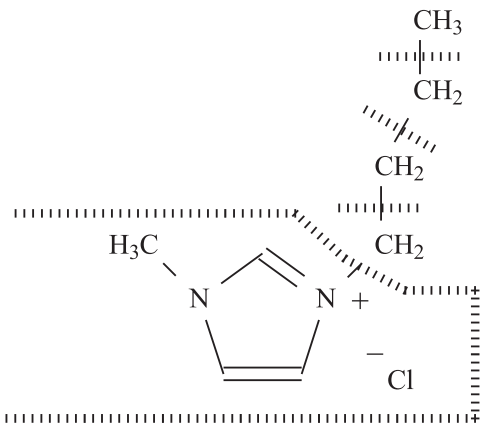


Fig. 5. Group segmentation of ionic liquid [BMIM]Cl.

various compositions and temperatures. The new parameters are suitable for ILs based on seven kinds of anions, namely, Cl, Br, BF_4, DMP, DBP, $EtSO_4$, and TfO. Similarly, works have been carried out for HFC/IL binary systems [75] and NH_3/IL binary systems [79]. The new group interaction parameters are also listed in Table 7, which can be used to extend the evaluating and predicting range of HFC/IL and NH_3/IL systems for developing alternative working pairs.

2.5. Excess property criterion

Closely associated with γ_i, there is the summation relationship of G^E [84].

$$G^E = \sum_{i=1}^{N} x_i[\partial(nG^E)/\partial n_i]_{p,T,n_j} = RT\sum_{i=1}^{N} x_i \ln \gamma_i \tag{8}$$

For the refrigerant and IL binary systems, Eq. (8) can be written as

$$G^E = RT(x_1 \ln \gamma_1 + x_2 \ln \gamma_2) \tag{9}$$

where values of $\ln \gamma_1$ and $\ln \gamma_2$ can be determined by Eqs. (1)–(3) using experimental data or with the help of the UNIFAC model.

According to an analysis of the Flory–Huggins equation [101], when the attraction of heterogeneous molecules is stronger than that of homogeneous molecules, the value of G^E is less than zero. In other words, a negative value of G^E means the affinity between the species is relatively stronger.

Thus, for a binary system at given temperature and pressure, a negative G^E is beneficial for solute absorption, and the smaller the value of G^E is, the better the absorption effect will be. At given temperature and pressure, G^E is a continuous function of system composition, which may exist more than one extreme point. The extreme point of G^E presents the characteristic of thermodynamic properties of the system. Therefore, the extreme point of G^E is presented as another selection criterion for evaluating suitable absorbents [102,103]. Thus, at given temperature and pressure, a smaller value of the extreme point of G^E for the solute–absorbent binary system indicates a stronger absorbing ability of the absorbent.

To evaluate the solute–absorbent binary system, the criterion based on the analysis of the extreme point of G^E is called "the criterion of minimum extreme value of the G^E-x relationship". The criterion based on the analysis of the absorption potential of solute is called "the criterion of maximum value of the absorption potential". The former is a macroscopic trend analysis on the basis of relatively more data points, while the latter is a local state view that requires only a small amount of data. In the case pressed for available VLE data, the latter may be more convenient. However, the combination of two methods can be used to obtain more

Table 7
Group interaction parameters for the UNIFAC model.

a_{nm}	CH_2	H_2O	[MIM]$EtSO_4$	[MIM]Cl	[MIM]Br	[MIM]BF_4	[MIM]DMP	[MIM]DBP	[MIM]TfO	CHF	CHF_2	CHF_3	[MIM]PF_6	[MIM]Tf_2N	NH_3	[MIM]Ac
CH_2	0.0	1318.0[a]	225.992	390.864	9530.493	874.744	305.640	214.708	−215.185	527.08[b]	134.38[b]	156.08[b]	692.26[a]	400.89[a]	−423.600	680.000
H_2O	300.00[a]	0.0	−99.370	−493.625	110.266	−239.783	−413.875	−435.828	295.777							
[MIM] $EtSO_4$	322.837	−325.889	0.0												−89.590	
[MIM]Cl	337.327	−191.757		0.0												
[MIM]Br	5237.786	−566.029			0.0											
[MIM]BF_4	−182.974	−416.931				0.0					57.54	5327.76			−404.700	
[MIM]DMP	440.260	−377.121					0.0								−64.470	
[MIM]DBP	390.885	−9.631						0.0								
[MIM]TfO	1593.671	−541.622							0.0		159.50					
CHF	105.48[b]									0.0			71.49			
CHF_2	35.69[b]					347.38			−6.95		0.0	224.25[b]	235.77	76.76		
CHF_3	96.28[b]					267.65					−131.47[b]	0.0	−47.24	424.39		
[MIM]PF_6	401.54[a]									196.90	−121.43	581.10	0.0			
[MIM]Tf_2N	145.80[a]										47.15	−100.69		0.0		
NH_3	914.100		2.849			320.400	−45.550								0.0	−216.100
[MIM]Ac	1244.000														−388.000	0.0

[a] Ref. [99].
[b] Ref. [100].

comprehensive evaluation conclusions. In addition, for the criterion of minimum extreme value of the G^E-x relationship, the absolute value of minimum extreme value of the G^E is commonly marked as G^E_{max}.

As shown in Table 8 and Fig. 6, for refrigerant R32 absorption systems with absorbents [BMIM]PF_6, [BMIM]BF_4, [BMIM]TfO, and [EMIM]Tf_2N, the G^E_{max} of R32/[EMIM]Tf_2N binary system is at minimum, showing that [EMIM]Tf_2N has better ability to absorb the refrigerant R32.

Comparing data from the UNIFAC model with the experimental data listed in Table 8, the predicted trends of G^E_{max} are basically the same as the experimental trends of the y_i/x_i obtained by literature data. The assessment results obtained by the G^E_{max} of the system agree essentially with the experimental data analysis. For R32 species, the phase equilibrium ratio values of the R32/[EMIM]Tf_2N system is relatively smaller, demonstrating [EMIM]Tf_2N has better absorbing ability compared with other absorbents.

3. Researches of H_2O and IL systems

3.1. Vapor pressure

As presented above, excellent working pairs are generally non-ideal mixtures. The strong affinity of absorbent with refrigerant often leads to the lower saturated vapor pressure of solution than that of ideal solution. In other words, VLE behavior exhibits highly negative deviation from Raoult's law, which is used to describe the VLE behavior of ideal mixture. Therefore, the decrease in saturated vapor pressure of solution becomes a significant indicator for assessing the affinity between refrigerant and absorbent.

In recent years, many researchers have investigated the VLE of IL working pairs systems. Table 9 summarizes the VLE measurement of H_2O/IL systems in literatures.

For the VLE measurement of H_2O/IL systems, the most widely used method is the boiling point method. The principle is to precisely prepare a mixture with known composition, observe phase behavior in the equilibrium cell, determining the properties in equilibrium state, e.g., pressure and temperature.

In 2004, Kim et al. [43] measured the vapor pressure of the systems H_2O/[BMIM]Br, H_2O/[BMIM]BF_4, and H_2O/[HydeMIM]BF_4 (1-(2-hydroxyethyl)-3-methylimidazolium tetrafluoroborate). They proposed that these systems could be used in absorption heat pumps.

Experimental data showed that the vapor pressure of water decreased with IL addition, but the decreasing degree differed according to IL type and concentration. For imidazolium based ILs, the interaction with H_2O was influenced by the type of anion and the length of cationic alkyl side chain. Generally, a shorter cationic alkyl side chain leads to stronger hydrophilicity. Moreover, the influence of the anion was much more significant than that of the cationic side chain.

In recent years, researchers have studied the thermophysical properties of H_2O/phosphoric IL working pairs, such as [DMIM] DMP, [EMIM]DMP, 1-ethyl-3-methylimidazolium diethylphosphate ([EMIM]DEP), 1-ethyl-3-ethyl-imidazolium diethylphosphate ([EEIM] DEP), and 1-butyl-3-methylimidazolium dibutylphosphate ([BMIM] DBP). All these ILs have strong affinity with water, especially [DMIM] DMP. Dong [72], He [109], Kato [112], Wang [117], Zhao [118] et al. measured the vapor pressure of the H_2O/[DMIM]DMP system at different temperatures, pressures, and compositions. The data provide the foundation for calculating the absorption cycle, and confirming the potential of the H_2O/[DMIM]DMP system to be used as working pairs.

Based on the potential use of hydrophilic IL as absorbent species combined with H_2O to constitute alternative working pairs, Li et al. [76] chose [DMIM]Cl and 1-methyl-3-methylimidazolium tetrafluoroborate ([DMIM]BF_4) as additives, added them to traditional working pairs H_2O/LiBr and H_2O/LiCl, and explored the modification effect of IL on traditional working pairs. They determined the saturated vapor pressures of ternary systems at different temperatures and concentration ranges using the boiling point method.

The correlation method of VLE data generally includes two categories. First is methods only using equations of state, such as PR, SRK, BWR, MH. Second is methods simultaneously using equations of state and the activity coefficient model, such as models of Margules, Wilson, NRTL, UNIQUAC, UNIFAC.

For H_2O/IL systems, Doker and Gmehling [107] analyzed VLE data correlation of H_2O/[EMIM]Tf_2N and H_2O/[BMIM]Tf_2N systems using three kinds of activity coefficient models including Wilson, NRTL, and UNIQUAC. Results showed that NRTL and UNIQUAC models, commonly used to correlate non-electrolyte solutions, are also suitable for IL working pairs with good accuracy. Carvalho et al. [120] determined VLE data of H_2O combined respectively with 1-ethyl-3-methylimidazolium chloride ([EMIM]Cl), [BMIM]Cl, 1-hexyl-3-methylimidazolium chloride ([HMIM]Cl), and Choline Chloride ([$N_{111(2OH)}$]Cl), the NRTL model was also used to correlate with data and a good fit was obtained.

In addition, for binary and ternary systems containing H_2O and IL, Wang et al. [117] and Li et al. [76] adopted the Antoine equation to correlate VLE data, the equation is expressed as

$$log(p/kPa) = \sum_{i=0}^{4} [A_i + 1000B_i/(T/K - 43.15)]w^i \tag{10}$$

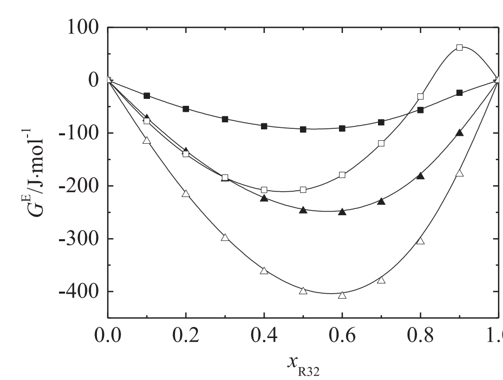


Fig. 6. G^E-x_{R32} for R32 systems at 298.20 K. ■, [BMIM]BF_4; □, [BMIM]TfO; ▲, [BMIM]PF_6; △, [EMIM]Tf_2N.

Table 8
The G^E_{max} for refrigerant R32 and IL binary systems at 298.20 K.

Refrigerant	IL		Experimental data				Cal. by UNIFAC
			T/K	P/MPa	y_i/x_i	Ref.	G^E_{max} /J·mol^{-1}
R32	[EMIM]Tf_2N	$C_8H_{11}F_6N_3O_4S_2$	298.15	0.399	3.077	[53]	−408.47
	[BMIM]PF_6	$C_8H_{15}F_6N_2P$	298.20	0.400	3.367	[54]	−250.77
	[BMIM]BF_4	$C_8H_{15}BF_4N_2$	298.20	0.400	3.676	[54]	−93.51
	[BMIM]TfO	$C_9H_{15}F_3N_2O_3S$	298.14	0.400	3.788	[73]	−207.90

Table 9
Summary of vapor pressure measurement for H_2O/IL systems.

IL	Measuring method	Ref.	Range of data	
			T/K	*p*/kPa
[BMIM]Cl	Dynamic recirculating still apparatus	[104]	373.15 – 441.11	101.3
[EMIM]$EtSO_4$	Dynamic recirculating still apparatus	[105]	373.15 – 410.58	101.3
[BMIM]MSO_4	Dynamic recirculating still apparatus	[106]	373.15 – 374.12	101.3
[EMIM]Tf_2N	Computer-driven static apparatus	[107]	353.15	3.193 – 47.422
[BMIM]Tf_2N			353.15	5.317 – 47.156
[DMIM]DMP	Boilling point method	[72]	302.57 – 441.87	2.14 – 101.01
[EMIM]Ac	Static apparatus	[108]	283.1 – 403.17	0.215 – 104.8
[HMIM]Cl			283.15 – 423.16	0.298 – 262.8
[DMIM]DMP	Boilling point method	[109]	329.35 – 429.75	6.62 – 39.15
[EEIM]DEP	Quasi-static ebulliometer method	[110]	317.63 – 371.31	9.313 – 57.075
[EMIM]BF_4	Gravimetric method	[111]	373.15 – 403.15	2.5 – 80.2
[BMIM]Br	Boilling point method	[43]	304.8 – 457.4	3.5 – 103.2
[BMIM]BF_4			311.4 – 475.2	3.5 – 102.6
[HydeMIM]BF_4			325.8 – 464.8	3.3 – 100.8
[DMIM]DMP	Computer-driven static apparatus	[112]	353.15	0.09 – 47.82
[EMIM]Tf_2N			353.15	3.19 – 47.39
[BMIM]Tf_2N			353.15	5.32 – 47.16
[EMIM]DMP	Bubble point method	[113]	320.35 – 411.15	6.27 – 43.56
[EMIM]TfO	Dynamic recirculating still apparatus	[114]	323.3 – 363.3	5.9 – 69.3
[EMIM]TFA			328.3 – 368.2	6.3 – 84.4
[EMIM]$EtSO_4$	Transpiration method	[115]	302.9 – 322.9	0.345 – 12.141
[EMIM]DMP	Quasi-static ebulliometer method	[116]	323.76 – 367.26	12.609 – 58.804
[DMIM]DMP	Quasi-static ebulliometer method	[117]	328.936 – 379.411	13.834 – 101.270
[DMIM]Cl	Boiling point method	[80]	287.15 – 437.45	1.10 – 100.98
[DMIM]BF_4	Boiling point method	[82]	312.25 – 403.60	4.69 – 103.23
[DMIM]DMP	Quasi-static ebulliometer method	[118]	312.88 – 373.01	6.937 – 79.824
[EMIM]DEP			324.01 – 373.26	11.872 – 83.919
[BMIM]DBP			317.98 – 368.07	9.184 – 81.630
[EMIM]$EtSO_4$	Boiling point method	[119]	320.35 – 373.35	4.21 – 24.75
[EMIM]Cl	Boiling point method	[120]	355.58 – 435.03	50 – 100
[BMIM]Cl			354.92 – 430.10	
[HMIM]Cl			354.64 – 405.30	
[$N_{111(2OH)}$]Cl			355.11 – 411.12	
[COC_2MOR][FAP]	Dynamic method	[121]	290.1 – 351.7	100
[COC_2MOR][Tf_2N]			291.0 – 349.6	
[COC_2PIP][FAP]			301.2 – 349.3	
[COC_2PIP][Tf_2N]			313.2 – 353.9	
[COC_2PYR][FAP]			307.4 – 351.6	
[COC_2PYR][Tf_2N]			291.8 – 357.5	
[BMPIP][$N(CN)_2$]			237.64 – 273.15	
[BMPYR][$N(CN)_2$]			236.26 – 273.15	
[BMPy][$N(CN)_2$]			244.19 – 300.30	
[BMPy][SCN]			238.03 – 273.15	

where *T* is the temperature, and *w* is the mass fraction of the absorbent. A_i and B_i are equation parameters obtained by regressing VLE data of the system.

3.2. Heat capacity

Heat capacity is an important factor affecting the coefficient of performance for absorption refrigeration cycles. A smaller heat capacity benefits heat transfer, reduces energy consumption, and improves the cycle performance. Measuring the constant pressure heat capacity enables the calculation of enthalpy, entropy, Gibbs free energy, and other thermodynamic functions. To discuss the relationship between the thermodynamic model of new working pairs and circulation mechanism, the heat capacity of new working pairs for absorption cycle must be studied.

Previous studies on the heat capacity determination of IL working pairs in literatures mainly focused on water or alcohol with IL systems, whereas the heat capacity of HFC or NH_3 with IL systems was rarely reported because of restricted test conditions. Table 10 summarizes researches on the heat capacity of H_2O/IL systems published in recent years.

Heat capacity is commonly measured by differential scanning calorimetry (DSC) and the micro-calorimeter method.

Table 10
Summary of heat capacity measurement for H_2O/IL systems.

System	Measuring method	Ref.	Range of *T*/K
H_2O/[DMIM]DMP	Calvet heat flow calorimeter	[72]	303.15 – 353.15
H_2O/[EMIM]$EtSO_4$	DSC	[122]	283.15 – 343.15
H_2O/[EMIM]TfO			283.15 – 343.15
H_2O/[EMIM]TFA			283.15 – 343.15
H_2O/[EMIM]$EtSO_4$	DSC	[123]	293.15 – 318.15
H_2O/[BMIM]CH_3SO_4			293.15 – 318.15
H_2O/[EMIM]TfO			293.15 – 318.15
H_2O/[BMIM]TfO			293.15 – 318.15
H_2O/[DMIM]DMP	Adiabatic solution calorimeter	[109]	298.15 – 323.15
H_2O/[EMIM]$EtSO_4$	DSC	[124]	303.2 – 353.2
H_2O/[EMIM]TfO			303.2 – 353.2
H_2O/[BMIM]CH_3SO_4	DSC	[125]	303.2 – 353.2
H_2O/[BMIM]TfO			303.2 – 353.2
H_2O/[BMIM]BF_4	DSC	[126]	278.15 – 333.15
H_2O/[EMIM]DMP	Adiabatic solution calorimeter	[113]	298.15 – 323.15
H_2O/[EMIM]$EtSO_4$	Isoperibol solution calorimeter	[119]	303.15 – 323.15

Heat capacity data in literatures are mostly correlated with temperature by a polynomial equation. A polynomial equation is then used to correlate the relationship of heat capacity with

temperature and composition.

$$C_p = \sum_{i=0}^{3} (a_i + b_i T) x^i \tag{11}$$

where C_p is the heat capacity. a_i and b_i are equation parameters obtained by regressing experimental data.

3.3. Density

As an important part of the fluid *PVT* data, liquid density plays a significant role in thermodynamics and is necessary for calculating other physical properties and studying of heat and mass transfer. In practice, the density of working pairs is closely related to temperature and composition, so the influence of the density change of a solution cannot be ignored when analyzing the absorption refrigeration cycle.

The density of most imidazolium based ILs roughly ranges within $1.1-1.6\ g/cm^3$, which is more important than that of water in practical applications. The density of IL mainly depends on the type of anion and cation, and the influence of anion is more obvious. Generally, a larger anion size leads to greater IL density, and a larger volume of organic cation leads to smaller IL density.

Previously studies on the density determination of IL working pairs in literatures mainly focused on water or alcohol with IL systems, whereas the density of HFC or NH_3 with IL systems was rarely reported because of restricted test conditions. Researches on the density of H_2O/IL systems in recent years are summarized in Table 11.

Density is commonly measured by the pycnometer [127,128], gravity balance (Westphal) [109,119,129,130], and vibrating U-tube densimeter [74, 131–139]. The vibrating U-tube densimeter method is one of the most common and highest accuracy methods to date. The uncertainty can reach $\pm 1 \times 10^{-6}\ g\ cm^{-3}$, and the measurement error does not exceed 0.005%. The working principle is to change the inherent oscillation frequency of the vibrating tube with the mass change (i.e., the density change) of the liquid flowing through the vibrating tube. After determining the relation between the oscillation period of the vibrating tube and liquid density, the density can be directly measured.

Solution density can be correlated with composition and temperature by various expressions. Given that the density of the IL solution has a simple relation with temperature and composition, a polynomial equation is selected to regress the density data of H_2O/IL systems as

$$\rho = \sum_{n=0}^{i} A_n w^n + T \sum_{n=0}^{i} B_n w^n + T^2 \sum_{n=0}^{i} C_n w^n \tag{12}$$

where ρ is the density of the binary system, w is the mass fraction of water. A_n, B_n and C_n are polynomial parameters obtained by fitting experiment data through the least square method.

Table 11
Summary of density measurement for H_2O/IL systems.

System	Measuring method	Ref.	Range of *T*/K
H_2O/[BMIM]N(CN)$_2$	Vibrating tube densimeter	[131]	278.15–363.15
H_2O/[BMIM]C(CN)$_3$			278.15–363.15
H_2O/[DMIM]Cl	Vibrating tube densimeter	[74]	293.15–318.15
H_2O/[BMIM]Br	Vibrating tube densimeter	[132]	298.15
H_2O/[DMIM]Br			298.15
H_2O/[EMIM]EtSO$_4$	Vibrating tube densimeter	[123]	293.15–318.15
H_2O/[BMIM]CH$_3$SO$_4$			293.15–318.15
H_2O/[EMIM]TfO			293.15–318.15
H_2O/[BMIM]TfO			293.15–318.15
H_2O/[BMIM]Cl	Vibrating tube densimeter	[133]	298.15–343.15
H_2O/[HMIM]Cl			298.15–343.15
H_2O/[OMIM]Cl			298.15–343.15
H_2O/[EMIM]EtSO$_4$	Vibrating tube densimeter	[134]	298.15–328.15
H_2O/[BMIM]CH$_3$SO$_4$	Vibrating tube densimeter	[135]	298.15–328.15
H_2O/[DMIM]DMP	Gravity balance	[109]	298.15–323.15
H_2O/[BMIM]Cl	Density bottle	[136]	298.15
H_2O/[EMIM]Br			298.15
H_2O/[BMIM]Br			298.15
H_2O/[BMIM]BF$_4$			298.15
H_2O/[EMIM]EtSO$_4$	Westphal balance	[129]	278.15–333.15
H_2O/[EMIM]BF$_4$	Vibrating tube densimeter	[137]	298.15
H_2O/[BMIM]BF$_4$			298.15
H_2O/[HMIM]BF$_4$			298.15
H_2O/[EMIM]EtSO$_4$	Vibrating tube densimeter	[138]	278.15–348.15
H_2O/[EMIM]TfO			278.15–348.15
H_2O/[EMIM]TFA			278.15–348.15
H_2O/[EMIM]BF$_4$	Vibrating tube densimeter	[95]	298.15
H_2O/[BMIM]BF$_4$			298.15
H_2O/[HMIM]BF$_4$			298.15
H_2O/[BMIM]PF$_6$			298.15
H_2O/[BMIM]DCA			298.15
H_2O/[EMIM]BF$_4$	Vibrating tube densimeter	[139]	298.15
H_2O/[EMIM]EtSO$_4$			298.15
H_2O/[EMIM]EtSO$_4$	Westphal balance	[130]	278.2–338.2
H_2O/[EMIM]BF$_4$	Pycnometer	[127]	293.15–323.15
H_2O/[BMIM]BF$_4$	Pycnometer	[128]	303.15–353.15
H_2O/[EMIM]EtSO$_4$	Gravity balance	[119]	303.15–323.15

3.4. Other properties

For a detailed investigation of the suggested working pairs, more properties such as viscosity, surface tension, and thermal conductivity are required.

The viscosity of IL working pair systems was rarely reported in literatures. The studied systems are mainly H_2O/[EMIM]BF$_4$, H_2O/[BMIM]BF$_4$, H_2O/[HMIM]BF$_4$, H_2O/[BMIM]Cl, H_2O/[EMIM]Br (1-ethyl-3-methylimidazolium bromide), H_2O/[BMIM]Br, H_2O/[EMIM]EtSO$_4$ (1-ethyl-3-methylimidazolium ethylsulfate), H_2O/[BMIM]MeSO$_4$ (1-butyl-3-methylimidazolium methylsulfate), and so on. Results show that the viscosity of H_2O/IL systems gradually decreases with the increasing water content. The viscosity of IL is generally tens to hundreds times higher than that of water mainly because of the different degrees of IL aggregation, due to the strong hydrogen bond between anion and cation. When water is added to IL, the hydrogen bond between the anion and cation weakens, which increases the mobility of ions and decreases the viscosity of IL.

The surface tension of IL is between that of water and common solvent, and decreases with the increase of temperature. However, the surface tensions of the refrigerant/IL systems are still rarely reported. The systems conducting research on surface tension include H_2O/[EMIM]BF$_4$, H_2O/[BMIM]BF$_4$, H_2O/[HMIM]BF$_4$, H_2O/[BMIM]Cl, H_2O/[BMIM]Br, H_2O/[EMIM]Br, and so on. The addition of IL can reduce the surface tension of the refrigerant quickly, which is beneficial to application in absorption refrigeration cycle.

The reports on the thermal conductivity of IL working pair systems which is necessary for the design of heat-transfer equipment are limited. The thermal conductivities for the binary systems H_2O/[EMIM]EtSO$_4$, H_2O/[DMIM]DMP, CH_3OH/[DMIM]DMP, and C_2H_5OH/[EMIM]EtSO$_4$ were reported. It is expected that refrigerant/IL systems could be perfect heat-transfer fluids.

Moreover, properties such as toxicity, environmental impact, and cost have to be evaluated and considered for further investigation.

4. Researches of other refrigerant and IL working pair systems

4.1. NH_3 and IL systems (solubility and other properties)

Because of the good mutual solubility of NH_3 and H_2O and the great latent heat of evaporation, the NH_3/H_2O working pair is widely used in various kinds of absorption refrigeration cycles. However, the system has some drawbacks such as high working pressure, toxicity, and difficulty in regenerating NH_3 from H_2O.

Table 12
Summary of solubility measurement of NH_3/IL systems.

Ionic liquid	Measuring method	Ref.	Range of *T*/K	Range of *p*/MPa	Range of *x*/mol%
[BMIM]PF_6	Static method	[23]	283.4 – 355.8	0.138 – 2.700	23.9 – 86.2
[HMIM]Cl			283.1 – 347.9	0.044 – 2.490	6.0 – 83.7
[EMIM]Tf_2N			283.3 – 347.6	0.114 – 2.860	4.5 – 94.8
[BMIM]BF_4			282.2 – 355.1	0.091 – 2.570	6.8 – 84.4
[EMIM]Ac	Static method	[50]	282.5 – 348.5	0.321 – 2.891	47.3 – 87.7
[EMIM]$EtSO_4$			282.7 – 372.3	0.287 – 4.777	42.4 – 87.5
[EMIM]SCN			283.2 – 372.8	0.244 – 5.007	34.0 – 87.6
[DMEA]Ac			283.2 – 372.8	0.136 – 4.249	45.4 – 86.5
[EMIM]BF_4	Static method	[140]	293.15 – 333.15	0.11 – 0.63	11.85 – 69.21
[BMIM]BF_4			293.15 – 333.15	0.07 – 0.83	6.08 – 75.31
[HMIM]BF_4			293.15 – 333.15	0.14 – 0.71	12.80 – 75.43
[OMIM]BF_4			293.15 – 333.15	0.10 – 0.61	13.21 – 80.81
[DMIM]DMP	Isothermal synthetic	[78]	293.15 – 333.15	0.053 – 0.665	7.0 – 75.2
[BMIM]Zn_2Cl_5	Static method	[141]	323.15 – 563.15	0.067 – 1.965	83.62 – 94.67

Therefore, a great number of new absorbents including IL have been studied as alternatives.

To find novel working pairs containing NH_3 as refrigerant and IL as absorbent, researchers have carried out related works. The research progress of VLE of NH_3/IL systems is presented in Table 12. The common method of determining the VLE data of NH_3/IL systems is as follows. First a certain mass of IL is added to the static equilibrium cell that is then filled with a certain mass of NH_3. Second the equilibrium cell is placed in a thermoregulated system (oil or water bath). The temperature and pressure are recorded when the NH_3/IL system reaches equilibrium at constant temperature. Third the equilibrium pressures at different temperatures are recorded by varying the temperature. Finally an appropriate model is used to calculate and obtain $p-T-x$ data. Using these experimental data, researchers can then verify the applicability of the thermodynamic model to NH_3/IL working pairs, simulate the working condition of the absorption cycle, and explore the prospects of the working pairs in practical applications.

As shown in Table 12, Yokozeki et al. [23,50] pioneered works in this region. They found that solubility of NH_3 in ILs such as [HMIM]Cl and [BMIM]PF_6 at 298 K is almost equivalent to that in water, i.e., negative deviations from Raoult's law for the two systems are at relatively the same level. Another important result is that NH_3 does not react with ILs under the experimental condition, and no loss of solvent occurs even in the acid solvent [HMIM]Cl. However, no absorption mechanism between NH_3 and various ILs is proposed and further study is deserved at the molecular level by spectroscopy methods.

In another work, Yokozeki [50] calculated residual properties such as residual enthalpy, residual entropy, and residual Gibbs energy of NH_3/IL systems. They found that these residual properties are all negative. The negative value of the NH_3/[DMEA]Ac system was the maximum, and residual properties of this system were close to those of the NH_3/H_2O system, indicates that a strong interaction like hydrogen bond exists between NH_3 and ILs.

In 2010, Li et al. [140] determined the VLE data of NH_3 and four ILs [C_nMIM]BF_4 (n=2, 4, 6, and 8) and studied the effect of alkyl side chain length of ILs on NH_3 absorption. Results show that the solubility of NH_3 in studied ILs is high and increases with the increase of alkyl side chain length. They believed that increase of carbon chain length leads to the decrease of ILs density, generating more free volume, and dissolving more NH_3 molecules. Using the Krichevisky–Kasarnovsky equation, Li et al. [140] calculated the Henry's constant and partial molar volume of NH_3, they established a thermodynamic model to calculate the enthalpy, entropy, Gibbs energy, and heat capacity of the system. Results confirm the non-spontaneity of the absorption process and the disadvantage of high temperature in NH_3 absorption.

Chen et al. [141] measured total pressures of NH_3 and metal ion-containing IL [BMIM]Zn_2Cl_5 by a static method, and correlated experimental data by the modified UNIFAC model. The solubilities of NH_3 in [BMIM]Zn_2Cl_5 is higher than that in the other ILs tested by Yokozeki et al. [50], but lower than that in $ZnCl_2$. Author's group [78] chose NH_3 and [DMIM]DMP as working pairs and determined solubilities by the isothermal synthesis method. The solubility decreases with increased temperature and increases with increased pressure. The experimental data are consistent with the calculated results from the NRTL model, with a relative deviation within 5%.

The literature survey reveals that properties of NH_3/IL working pairs have been gradually examined in recent years. Given the controllability of the IL structure (i.e., various ILs can be synthesized according to a given target or practical needs), the gap in this applied research field urgently needs to be filled. Moreover, considering the high solubility and low energy consumption in the separation of NH_3/IL systems, it is necessary to study the interaction between NH_3 and various ILs, for the development of suitable working pairs for absorption cycle.

4.2. HFCs and IL systems (solubility and other properties)

As a kind of refrigerant, HFCs are also concerned in developing novel absorption IL working pairs. The research progress of the VLE of HFC/IL systems is summarized in Table 13. The studied refrigerants are tetrafluoromethane (R14), trifluoromethane (R23), R32, fluoromethane (R41), R125, R134, R134a, R152a, and fluoroethane (R161).

Shiflett and Yokozeki et al. [47,53,54,58,61,62] determined the solubility and diffusivity of HFCs such as R32, R134a, R125, R23, R152a, R134, and R161 in ILs by gravimetric microbalance, and used the EOS, NRTL, and Antoine-type equation to process the experimental data. Ren et al. [96] determined the solubility of R134a in [HMIM]-based ILs, regressed the experimental data using the PR EOS with van der Waals two-parameter mixing rules, and studied the effect of the anion and cationic carbon chain length on the solubility and molar volume of R134a in ILs. Author's group [73] determined the solubility of R32 and R152a in 1-ethyl-3-methylimidazolium trifluoromethanesulfonate ([EMIM]TfO) and [BMIM]TfO by the isothermal synthesis method, results well fit the NRTL model.

4.3. HC and IL systems (solubility and other properties)

Many researchers have studied the physical and chemical properties of HC and IL binary systems to discuss their potential use as working pairs of absorption cycle. Lee et al. [144] measured

Table 13
Summary of solubility measurement of HFC/IL systems.

Refrigerant	Absorbent	Measuring method	Ref.	Range of *T* /K	Range of *p*/MPa
R32	[EMIM]TfO	Isothermal synthetic	[73]	273.14 – 298.15	0.097 – 0.857
	[BMIM]TfO			273.13 – 298.19	0.104 – 0.902
R152a	[EMIM]TfO			273.16 – 348.17	0.040 – 0.848
	[BMIM]TfO			273.22 – 348.15	0.056 – 0.879
R14	[HMIM]Tf_2N	Synthetic method	[142]	293.3 – 413.3	1.202 – 9.582
R134a	[HMIM]Tf_2N	Static method	[96]	398.15 – 348.15	0.042 – 4.320
	[HMIM]PF_6				0.081 – 14.330
	[HMIM]PF_6				0.081 – 12.880
R23	[EMIM]PF_6	Synthetic method	[143]	308.17 – 367.33	1.602 – 51.64
R32	[BMIM]PF_6	Gravimetric microbalance	[54]	283.2 – 348.2	0.0097 – 0.9999
	[BMIM]BF_4			283.0 – 348.2	0.0097 – 0.9999
R125	[BMIM]PF_6			283.1 – 348.3	0.0099 – 0.9998
R134a	[BMIM]PF_6			283.0 – 348.2	0.0097 – 0.3500
R23	[BMIM]PF_6			282.6 – 348.1	0.0098 – 2.0002
R152a	[BMIM]PF_6			283.1 – 348.2	0.0097 – 0.4505
R32	[DMPIM]TMeM	Gravimetric microbalance	[53]	283.15 – 348.15	0.0094 – 1.0005
	[EMIM]BEI			283.15 – 348.05	0.0096 – 1.0005
	[DMPIM]BMeI			298.15	0.0099 – 1.0011
	[EMIM]BMeI			283.15 – 348.05	0.0096 – 1.0005
	[Pmpy]BMeI			283.15 – 348.05	0.0095 – 1.0004
	[bmpy]BMeI			298.15	0.0096 – 1.0000
	[BMIM]Ac				0.0099 – 1.0004
	[BMIM]SCN				0.0095 – 0.9992
	[BMIM]$MeSO_4$				0.0099 – 1.0006
	[EMIM]TFES				0.0099 – 1.0016
	[BMIM]TFES				0.0097 – 0.9989
	[HMIM]TFES				0.0099 – 0.9980
	[DMIM]TFES				0.0096 – 1.0010
	[BMIM]HFPS				0.0095 – 1.0004
	[BMIM]FS				0.0100 – 1.0005
	[BMIM]TPES				0.0095 – 0.9994
	[BMIM]TTES				0.0095 – 0.9992
R134a	[EMIM]BEI	Gravimetric microbalance	[62]	283.10 – 348.10	0.0103 – 0.3505
	[BMIM]HFPS			283.10 – 348.10	0.0099 – 0.3506
	[BMIM]TPES			283.05 – 348.10	0.0102 – 0.3505
	[BMIM]TTES			283.10 – 348.15	0.0102 – 0.3505
	[6,6,6,14-P]TPES			282.90 – 348.10	0.0098 – 0.3504
	[4,4,4,14-P]HFPS			283.05 – 348.10	0.0099 – 0.3504
R41	[BMIM]PF_6	Gravimetric microbalance	[58]	283.09 – 348.18	0.0097 – 1.9995
R161	[BMIM]PF_6			283.06 – 348.16	0.0099 – 0.7005
R134	[BMIM]PF_6			283.11 – 348.16	0.0101 – 0.3505
R134	[EMIM]Tf_2N	Gravimetric microbalance	[47]	282.9 – 348.1	0.0099 – 0.3505
R125	[EMIM]Tf_2N	Gravimetric microbalance	[61]	283.1 – 348.2	0.0100 – 0.9998
R134a	[EMIM]Tf_2N			282.7 – 348.1	0.0100 – 0.3503

solubility data of various HCs in [BMIM]Tf_2N by the saturation method and obtained Henry's constant through the experimental data. Shiflett et al. [47,60,61] determined the solubility data of a series of HCs and fluorinated benzene in [EMIM]Tf_2N using the gravimetric microbalance and volumetric method, then experiment data were correlated with the NRTL model. Liu et al. [145,146] predicted solubilities of small HCs in about 700 ILs, and reported solubilities of methane, ethane, ethylene and propane in trimethyloctylphosphonium bis(2,4,4-trimethylpentyl) phosphinate ([P8111]TMPP), tetrabutylphosphonium bis(2,4,4-trimethylpentyl)phosphinate ([P4444]TMPP) and [EMIM]Tf_2N. Table 14 summarizes studies on the VLE of HC/IL systems published in recent years.

4.4. Alcohol and IL systems (solubility and other properties)

Kim et al. [42] determined the solubility data of TFE in [BMIM]Br and [BMIM]BF_4 by the boiling point method and correlated the data with the Antoine-type equation. Shiflett et al. [56] determined the VLE data of the *n*-butanol/[BMIM]PF_6 system using the volumetric method. Verevkin [148], Zhao [118], Wang [116], Jiang [110], Wang [80,117], Shen [149] and Carvalho et al. [120] determined the VLE data of alcohols and benzene in different ILs by the static method, correlated the data using NRTL, Antoine-type and other equations, and obtained the activity coefficients and model parameters of different solutes in ILs. González et al. [150] determined vapor pressure of four alcohols in 1-hexyl-3-methylimidazolium trifluoromethanesulfonate ([HMIM]TfO) using the vapor pressure osmometry technique and derived other thermodynamic properties. Particularly, Zhang et al. [151] proposed a new alternative working pairs for absorption refrigeration cycle, which was ternary solutions H_2O/CH_3OH(or C_2H_5OH)/[BMIM]DBP, and measured vapor pressure of binary solutions H_2O(CH_3OH, orC_2H_5OH)/[BMIM]DBP with an inclined boiling apparatus to obtain binary interaction parameters of NRTL activity coefficient model, then measured and predicted vapor pressure of proposed solutions with the same apparatus and model. Studies on the VLE, density, heat capacity, and viscosity of alcohol and IL systems published in recent years are listed in Tables 15–18.

5. Assessment of absorption cycle adopting IL working pairs

5.1. Simulation for single-effect absorption cooling cycle

To determine whether a working pair has the potential for further research and development, it should be placed in an

Table 14
Summary of solubility measurement of HC/IL systems.

Refrigerant	Absorbent	Measuring method	Ref.	Range of *T* /K	Range of *p* /kPa
Propane	[BMIM]Tf$_2$N	Saturation method	[144]	279.98 – 339.97	88.3 – 1062.2
Propene					999 – 1218.2
Butane				280.00 – 340.00	334 – 304.1
1-Butane					21.0 – 351.1
Hexane	[BMIM]TfO	Static apparatus	[147]	363.15	15.79 – 165.7
1-Hexane					22.54 – 180.9
2,2,4-Trimethylpentane					11.86 – 65.21
1-Nonene					2.599 – 16.34
Decane					2.000 – 6.202
1-Decane					1.132 – 6.989
1-Hexane	[OMIM]TfO				16.19 – 198.8
1-Octene					1.672 – 30.24
1-Nonene					0.784 – 13.45
Fluorinated benzenes	[EMIM]Tf$_2$N	Volumetric method	[60]	282.5 – 373.0	–
Benzene	[BMIM]Tf$_2$N	Static method	[148]	298.15 – 313.15	0 – 24.331
Methane	[P8111]TMPP	Isochoric saturation method	[145,146]	299 – 323	1090 – 3610
Ethane					540 – 1690
Ethylene					1080 – 3540
Propane					50 – 210
Methane	[P4444]TMPP			313 – 353	0 – 5000
Ethane					
Ethylene					
Propane					
Methane	[EMIM]Tf$_2$N			299 – 354	0 – 4000
Ethane					
Ethylene					
Propane					

Table 15
Summary of vapor pressure measurement of alcohol/IL systems.

Refrigerant	Absorbent	Measuring method	Ref.	Range of *T* /K	Range of *p*/kPa
Ethanol	[EMIM]TOS	Ebulliometric method	[152]	373.15	0.0533 – 0.2250
Methanol	[EEIM]DEP	Quasi-static method	[110]	299.20 – 366.19	14.336 – 65.452
Ethanol	[EEIM]DEP			309.80 – 370.80	9.139 – 56.716
Methanol	[EMIM]DMP	Bubble point method	[113]	301.95 – 386.15	0.01134 – 0.04630
Ethanol				309.05 – 389.15	0.00747 – 0.05110
Methanol	[DMIM]Cl	Quasi-static method	[149]	298.85 – 348.63	16.65 – 102.57
Ethanol	[DMIM]Cl			312.19 – 361.04	11.54 – 101.90
1-Butanol	[BMIM]PF$_6$	Volumetric method	[56]	285.7 – 332.0	–
Methanol	[BMIM]Tf$_2$N	Static method	[148]	298.15 – 313.15	0 – 35.450
Ethanol	[BMIM]Tf$_2$N				0 – 17.928
Propanol	[BMIM]Tf$_2$N				0 – 6.986
Methanol	[EMIM]DMP	Quasi-static method	[116]	299.20 – 343.86	15.969 – 60.419
Ethanol	[EMIM]DMP			309.95 – 350.67	14.165 – 60.073
1-Propanol	[DMIM]DMP	Quasi-static method	[117]	330.478 – 401.916	11.094 – 100.935
2-Propanol	[DMIM]DMP			316.402 – 384.177	11.149 – 102.082
TFE	[BMIM]Br	Boiling-point method	[42]	293.2 – 469.4	0.0049 – 0.1010
	[BMIM]BF$_4$			315.2 – 469.4	0.0068 – 0.1003
	[EMIM]BF$_4$	Boiling-point method	[80]	283.15 – 460.85	0.00306 – 0.10102
Methanol	[DMIM]DMP	Quasi-static method	[118]	285.96 – 343.71	7.811 – 76.224
	[EMIM]DEP			285.31 – 342.19	7.943 – 79.563
	[BMIM]DBP			286.82 – 335.10	8.431 – 80.194
Ethanol	[DMIM]DMP			298.62 – 359.57	7.853 – 74.249
	[EMIM]DEP			302.30 – 356.00	9.068 – 81.091
	[BMIM]DBP			298.42 – 355.12	7.606 – 77.658
Ethanol	[EMIM]Cl	Boilling point method	[120]	334.80 – 392.42	50 – 100
	[BMIM]Cl			335.03 – 405.89	
	[HMIM]Cl			335.15 – 411.86	
	[N$_{111(2OH)}$]Cl			334.99 – 353.06	
H_2O/CH_3OH	[BMIM]DBP	Boiling-point method	[151]	315.95 – 392.65	11.34 – 72.02
H_2O/C_2H_5OH				321.65 – 395.65	11.76 – 69.02
1-Propanol	[HMIM]TfO	Vapor pressure osmometry technique	[150]	323.15	10.39 – 12.07
2-Propanol					20.12 – 23.52
1-Butanol					3.89 – 4.46
2-Butanol					8.85 – 10.56
1-Pentanol					1.44 – 1.63

absorption cycle to assess the performance by simulation or experiment. Some researchers have carried out such works, but the main method is still limited to simulation and analysis on the basis of thermophysical properties of the IL working pairs. The works mainly focus on single-effect absorption cooling cycle.

Table 16
Summary of density measurement of alcohol/IL systems.

Refrigerant	Absorbent	Measuring method	Ref.	Range of *T*/K
Ethanol Methanol	[DMIM]DMP	Gravity balance	[109]	298.15–323.15
Methanol	[OMIM]Cl	Vibrating tube densimeter	[153]	298.15–328.15
Methanol	[EMIM]DMP [BMIM]DMP	Vibrating tube densimeter	[154]	293.15–333.15
Ethanol	[EMIM]DMP [BMIM]DMP			
Ethanol	[EMIM]HS [EMIM]OS [EMIM]ES [EMIM]BS	Viscodensimeter	[155]	288–318
Ethanol	[EMIM]Tf_2N	Density meter	[156]	293.15–323.15

Table 17
Summary of heat capacity measurement of alcohol/IL systems.

Refrigerant	Absorbent	Measuring method	Ref.	Range of *T*/K
Ethanol Methanol	[DMIM]DMP	Adiabatic solution calorimeter	[109]	298.15–323.15
Ethanol Methanol	[EMIM]DMP	Adiabatic solution calorimeter	[113]	298.15–323.15
Methanol Methanol	[HMIM]BF_4 [OMIM]BF_4	DSC	[157]	283.15–323.15

Table 18
Summary of viscosity measurement of alcohol/IL systems.

Refrigerant	Absorbent	Measuring method	Ref.	Range of *T*/K
Ethanol Methanol	[DMIM]DMP	Capillary viscometer	[109]	298.15–323.15
Methanol	[OMIM]Cl	Capillary microviscosimeter	[153]	298.15–328.15
Methanol	[EMIM]DMP [BMIM]DMP	Micro viscometer	[154]	293.15–333.15
Ethanol	[EMIM]DMP [BMIM]DMP			
Ethanol	[EMIM]Tf_2N	Viscosity meter	[156]	293.15–323.15

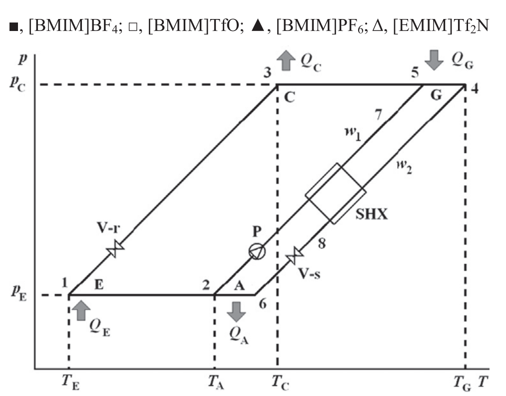


Fig. 7. Schematic of the single-effect absorption cooling cycle.

The single-effect absorption cooling cycle consists of an evaporator E, a condenser C, a generator G, an absorber A, and a solution heat exchanger SHX, whose schematic is shown in Fig. 7. 1–2–5–3–1 represents the refrigerant circulation loop, and 6–2–5–4–6 is the solution circulation loop. In the cycle calculation, mass transfer, heat transfer, and resistance loss in the solution flow process are neglected. Therefore, both positive and reverse cycles can be considered as ideal cycles, with the highest efficiency of heat transfer and cooling properties.

In the refrigerant circulation loop, the generator is heated by Q_G and separates high-pressure refrigerant vapor 5. The vapor refrigerant then enters the condenser, liquefies into liquid refrigerant 3, and releases heat Q_C. The high-pressure liquid refrigerant passes through an expansion valve and goes into the evaporator. In the evaporator, the liquid refrigerant is vaporized and the cooling load Q_E is produced.

In the solution circulation loop, the low-pressure vapor refrigerant 1 from the evaporator is absorbed in the absorber by the rich solution 8 concentrated in the generator and then releases heat Q_A. The pressure of the poor solution 2 leaving the absorber is enhanced after pumping, and then the poor solution is supplied to the generator. In the generator, the poor solution is heated up to boiling by the low-grade heat source, and the refrigerant is vaporized and separated from the solution. The rich solution 4 desorbing the refrigerant reduces the pressure through the expansion valve and flows back to the absorber.

To simplify the computer simulation of a cycle, following assumptions are made. The pressures of the condenser and the generator are equal ($p_C = p_G$), and the pressures of the absorber and evaporator are equal ($p_A = p_E$). The connecting pipeline has no pressure drop. Compared with other forms of thermal power, the pumping work is so small that is usually ignored. The refrigerant expansion process from the condenser to the evaporator is isenthalpic, and the temperature of evaporator outlet is the dew point of the pure refrigerant. The flow rate of vapor refrigerant is

set to $1\ \text{kg s}^{-1}$, and the vapor of absorbent is ignored, etc. [158,159].

According to the above assumptions, if the refrigerant vapor generated in the evaporator is $1\ \text{kg s}^{-1}$, the heat added to the evaporator is (h_3+Q_E), and the heat leaving the evaporator is h_2. Based on the energy balance, the cooling capacity Q_E of single-effect absorption cooling cycle is

$$Q_E = h_2 - h_1 \quad (13)$$

where h_1 is the enthalpy of stream 1 in Fig. 7, h_2 is the enthalpy of the saturated refrigerant vapor at evaporation pressure.

In the generator, when per unit mass (e.g., 1 kg) of refrigerant vapor is produced, f kg poor solution is needed to flow into the generator. The value of f is called the circulation ratio. Conversely, if the poor solution flowing into the generator is f kg, 1 kg refrigerant vapor is produced in the generator. Therefore, the rich solution leaving the generator is $(f-1)$ kg. The pure absorbent almost has no vapor pressure, i.e., the pure absorbent in the stream inflow and outflow of the evaporator remains the same based on the mass balance,

$$f w_p = (f-1) w_r \quad (14)$$

or

$$f = w_r/(w_r - w_p) \quad (15)$$

where w_p is the mass fraction of the absorbent in poor solution, w_r is the mass fraction of the absorbent in rich solution.

Investigating the heat into and out of the generator, the heat added to the generator is Q_G+fh_3, and the heat leaving the generator is $(f-1)h_4+h_5$, thus

$$Q_G = (f-1)h_4 + h_5 - fh_3 \quad (16)$$

The performance of absorption refrigeration cycle is characterized by the coefficient of performance defined as

$$COP = Q_E/Q_G = (h_2-h_1)/[h_5+f(h_4-h_3)-h_4] \quad (17)$$

where h_i represents the enthalpy of stream i (kJ kg^{-1}). The enthalpy of each state point can be calculated on the basis of thermodynamic properties of refrigerant or IL working pair.

The above analysis reveals that *COP* determination is based on the enthalpy of stream. In principle, the enthalpy of stream is the state function on the temperature, pressure, and composition of a given stream. In fact, Fig. 7 is also a phase diagram of the binary system. Using Fig. 7, the calculation method can be explained by the fact that the state of each point in the cycle needs to be determined, and then the enthalpy can be calculated based on the state. For example, based on the heat source temperature T_G, the pressure and composition of stream in the generator can be determined. Generally, the enthalpy of a multi-component fluid is

$$h = \sum x_j h_j + \Delta_{mix} h \quad (18)$$

or

$$h = \sum x_j \int_{T_0}^{T} C_{p,j}\, dT + \Delta_{mix} h \quad (19)$$

where $C_{p,j}$ is the heat capacity of species j of stream, $\Delta_{mix}h$ is the mixing enthalpy of the system, which is usually ignored. T_0 is the reference temperature, usually treated as 298.15 K.

5.2. Performance assessment of absorption cycles

Table 19 lists the published *COP* of refrigerant/IL systems for single-effect absorption cooling cycle. Deviations among the calculated results exist because different calculations are based on different property data, thermodynamic models, and operating conditions, e.g., heat source temperature.

Table 19
COP of refrigerant/IL systems for single-effect absorption cooling cycle.

System	Ref.	T_E/°C	T_A/°C	T_C/°C	T_G/°C	f	*COP*
H_2O/[BMIM]BF_4	[49]	10	30	40	100	13.0	0.544
H_2O/[EMIM]BF_4						18.2	0.525
H_2O/[EMIM]$EtSO_4$						13.57	0.569
H_2O/[DMIM]DMP						5.32	0.662
H_2O/[BMIM]I						23.7	0.534
H_2O/[BMIM]DBP						11.17	0.532
H_2O/[EEIM]DEP						12.38	0.565
H_2O/[EMIM]DEP						7.75	0.588
H_2O/[EMIM]DMP						8.66	0.691
H_2O/[DMIM]DMP	[72]	10	30	40	80	8.77	0.829
H_2O/[DMIM]Cl						9.54	0.827
CH_4O/[DMIM]DMP	[66]	10	30	40	100	3.71	0.87
TFE/[BMIM]Br	[81]	10	30	40	80	4.39	0.807
TFE/[BMIM]BF_4						6.07	0.780
TFE/[EMIM]BF_4						5.25	0.793
R22/[BMIM]BF_6	[46]	10	30	40	100	5.12	0.319
R32/[BMIM]BF_6						7.35	0.385
R32/[BMIM]BF_4						6.41	0.330
R134/[BMIM]BF_6						4.38	0.348
R134a/[BMIM]BF_6						10.66	0.254
R152a/[BMIM]BF_6						13.27	0.300
R125/[BMIM]BF_6						16.49	0.128
NH_3/[BMIM]BF_4	[23]	10	30	40	100	12.98	0.557
NH_3/[BMIM]BF_6						17.27	0.575
NH_3/[EMIM]Tf_2N						24.57	0.589
NH_3/[HMIM]Cl						14.26	0.525
NH_3/[EMIM]Ac	[50]	10	30	40	100	12.55	0.573
NH_3/[EMIM]$EtSO_4$						17.55	0.485
NH_3/[EMIM]SCN						12.42	0.557

To study the feasibility of NH_3/IL systems in industrial applications, Yokozeki et al. [50] calculated the performance of absorption cycle using NH_3/IL working pairs. In the studied imidazolium ILs, the cycle performance of [EMIM]Tf_2N as absorbent is the best, but the *COP* is slightly lower than that of the NH_3/H_2O system. Given that the distillation separation of the NH_3/[EMIM]Tf_2N system does not consume too much energy, the application of NH_3/[EMIM]Tf_2N system may be feasible.

Results in Table 19 show that the *COP* of H_2O/IL systems ranges within 0.52–0.83, which do not exceed the traditional H_2O/LiBr working pair. However, the *COP* of H_2O/[DMIM]DMP and H_2O/[DMIM]Cl systems are close and slightly lower than that of H_2O/LiBr. Particularly, the H_2O/[DMIM]DMP system overcomes the crystallization and corrosion problems of traditional working pair to some extent, and broadens the operating range. For HFC/IL systems, the *COP* ranges within 0.12–0.39, which are still relatively low but may be used in absorption/compression hybrid cycle. For NH_3/IL systems, the *COP* ranges within 0.48–0.59, which are lower than that of the traditional NH_3/H_2O working pair, but the difficulty of separation is relieved.

$$q_G = fC_p(T_G - T_{in}) + \Delta_{eva} h_{T_G} + \Delta_{mix} h \quad (20)$$

where q_G is the heat load of unit mass refrigerant produced in the generator, which consists of three parts. $fC_p(T_G-T_{in})$ expresses the heat needed to warm the supercooled solution from entering the generator to the generation temperature, $\Delta_{eva}h_{TG}$ is the latent heat of evaporation of the refrigerant at T_G, and $\Delta_{mix}h$ is the mixing heat of liquid refrigerant and absorbent. A larger f causes larger heat load of evaporator, thereby reducing the *COP* of the cycle.

Fig. 8 shows that with the increase of generation temperature, the *COP* of various working pairs sharply increases initially, then becomes stable, and slightly declines finally. f is infinite when the generation temperature reaches the minimum, the required generation heat is infinite based on Eq. (20), and the *COP* of the cycle is zero. With the increase of generation temperature f decreases, *COP* sharply increases and then smoothens. With further rise of

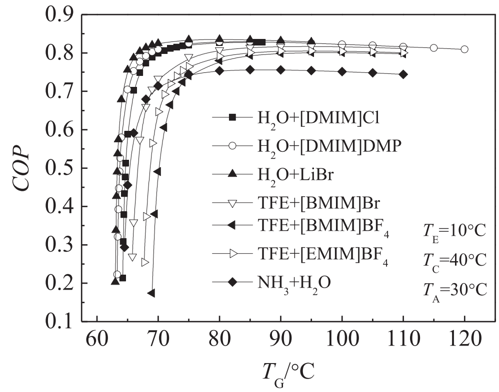


Fig. 8. *COP* of seven working pairs versus T_G for single-effect absorption cooling cycle.

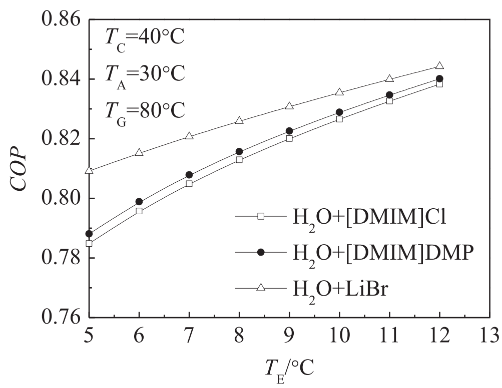


Fig. 9. Effect of T_E on *COP*.

generation temperature, the temperature difference ($T_G - T_{in}$) increases, the generated heat increases, and then the *COP* of the cycle slightly decreases. At the stationary stage, the working pairs consisting of TFE and three different ILs, whose *COP* ranges between those of H_2O/LiBr and NH_3/H_2O working pairs, have wider operating range. Among these working pairs, the *COP* of the TFE/[BMIM]Br system is the highest. At the stationary stage, the *COP* of H_2O/[DMIM]DMP and H_2O/[DMIM]Cl are close but slightly lower than that of the H_2O/LiBr working pair. Given that the H_2O/[DMIM]DMP system has no crystallization limits and has the widest operating range, the operational safety greatly improves. The operating range of the H_2O/LiBr system comes second, and the operating range of the H_2O/[DMIM]Cl system is the narrowest. As an absorbent, [DMIM]DMP has a higher solubility with the refrigerant, e.g., H_2O, and a higher boiling point than refrigerant. Simulation results also show that the H_2O/[DMIM]DMP system is expected to become an absorption cycle alternative working pair.

For two preferred suitable H_2O/IL systems H_2O/[DMIM]Cl and H_2O/[DMIM]DMP, the effects of evaporation temperature on the system *COP*, system exergy efficiency (η_E), and *f* are analyzed and compared with the traditional working pair H_2O/LiBr. Fig. 9 shows the effect of the evaporation temperature on the *COP*, which is found to follow the order H_2O/LiBr > H_2O/[DMIM]DMP > H_2O/[DMIM]Cl, and are all higher than 0.78. With the increase of evaporation temperature, the *COP* of the system increases, this is because that when the evaporation temperature is low, the corresponding evaporation pressure is low, *f* is high, and *COP* is low.

Fig. 10 shows the effect of the evaporation temperature on η_E. The effect of T_E on *COP* is opposite to that of η_E. *COP* increases with the increase of T_E, whereas η_E decreases with the increase of T_E.

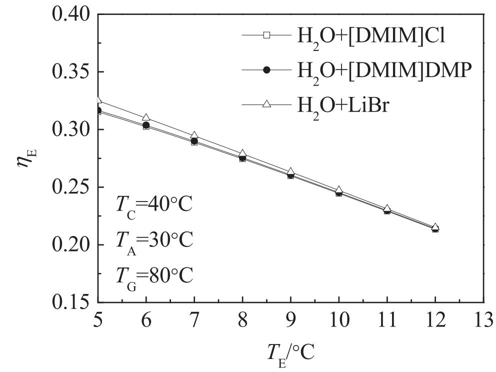


Fig. 10. Effect of T_E on η_E.

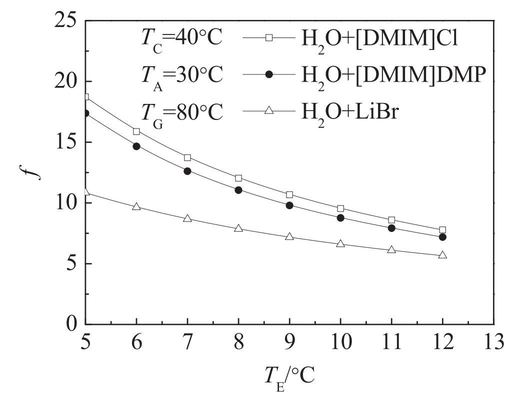


Fig. 11. Effect of T_E on *f*.

This is mainly because *COP* considers only the amount of cooling capacity, while the η_E considers not only the amount of cooling capacity but also the grade of cooling capacity. In other words, the cooling load and cooling temperature are all important for the absorption cooling cycle, a lower cooling temperature results in a higher grade of cold, so η_E decreases with the increase of T_E. Fig. 10 shows that for the three studied working pairs, η_E follows the order H_2O/LiBr > H_2O/[DMIM]DMP > H_2O/[DMIM]Cl.

Fig. 11 shows the effect of the evaporation temperature on *f*, *f* values of H_2O/[DMIM]Cl and H_2O/[DMIM]DMP systems are higher than that of the H_2O/LiBr system, and *f* decreases with the increase of evaporation temperature. *f* also markedly affects *COP*, increasing *COP* needs *f* to be reduced. To reduce *f*, the concentration difference ($w_r - w_p$) should be increased and the concentration of the rich solution should be reduced.

As summarized above, the mixture systems of refrigerant and IL are novel, environmental friendly absorption cycle working pairs. Thus, these systems are attracting increasing attentions, and further research and development are necessary.

6. Conclusions

The research frontiers of IL working pairs for absorption cycle in recent years were surveyed, to make the relevant work more rational and efficient. Based on macroscopic properties and intermolecular interactions, selection methods of IL as absorbent were introduced. In particular, based on the author's previous studies, from the perspective of action mechanism between absorbent and refrigerant, evaluation methods of combining the UNIFAC model with extreme G^E criterion were proposed, and the actual research achievements of the method were also presented. The research progresses of thermophysical properties of IL working pairs were

summarized, such as the test method, popular system, modeling of vapor pressure, solubility, heat capacity, and density. Based on thermophysical property investigations of H_2O, NH_3, alcohol, and HFC systems, as well as researches of ternary systems with IL added to the traditional working pairs, several potential binary and ternary systems were put forward. Finally, working performances of absorption cycle with IL working pairs were calculated and assessed to further validate the development potential of H_2O, NH_3, alcohol, and HFC working pairs.

Nomenclature

A_i and B_i parameters of Eq. (10) (dimensionless)
A_n, B_n and C_n parameters of Eq. (12) (dimensionless)
a, b, and c parameters of Eq. (3) (dimensionless)
a_i and b_i parameters of Eq. (11) (dimensionless)
CFC chlorofluorocarbon (dimensionless)
COP coefficient of performance (dimensionless)
C_p the heat capacity (kJ kg^{-1} K^{-1})
DBP dibutylphosphate (dimensionless)
DMEU N,N'-dimethylethyleneurea (dimensionless)
DMPU N,N′-dimethylpropyleneura (dimensionless)
DSC differential scanning calorimetry (dimensionless)
E181 tetraethylene glycol dimethyl ether (dimensionless)
EOS equation of state (dimensionless)
f circulation ratio (dimensionless)
G^E excess Gibbs function (kJ kg^{-1})
HC hydrocarbon (dimensionless)
HFC hydrofluorocarbon (dimensionless)
HFIP hexafluoroisopropanol (dimensionless)
h_i enthalpy of stream i in Fig. 7, i=1,2,...,5 (kJ kg^{-1})
IL ionic liquid (dimensionless)
k_1 Henry's constant of the refrigerant species (kPa)
NMP N-methyl-2-pyrrolidone (dimensionless)
p system pressure (kPa)
p_1^s saturated vapor pressure of the refrigerant species (kPa)
Q heat load (kW)
q heat load of unit mass refrigerant (kW kg^{-1})
R&D research and development (dimensionless)
R114 1,2-dichloro-1,1,2,2-tetrafluoroethane (dimensionless)
R125 pentafluoroethane (dimensionless)
R134 1,1,2,2-tetrafluoroethane (dimensionless)
R134a 1,1,1,2-tetrafluoroethane (dimensionless)
R14 tetrafluoromethane (dimensionless)
R143a 1,1,1-trifluoroethane (dimensionless)
R152a 1,1-difluoroethane (dimensionless)
R161 fluoroethane (dimensionless)
R23 trifluoromethane (dimensionless)
R32 difluoromethane (dimensionless)
R41 fluoromethane (dimensionless)
SHX solution heat exchanger (dimensionless)
T system temperature (K)
T_0 reference temperature (K)
TFE 2,2,2-trifluoroethanol (dimensionless)
T_{in} temperature of supercooled solution entering the generator (K)
VLE vapor–liquid equilibrium (dimensionless)
w mass fraction of the absorbate species (dimensionless)
x_i liquid phase mole fraction of species i (dimensionless), i=1, 2, 1 presents refrigerant, 2 presents absorbant
y_i vapor phase mole fraction of species i (dimensionless), i=1, 2, 1 presents refrigerant, 2 presents absorbant
[BMIM]BF_4 1-butyl-3-methylimidazolium tetrafluoroborate (dimensionless)
[BMIM]Br 1-butyl-3-methylimidazolium bromide (dimensionless)
[BMIM]Cl 1-butyl-3-methylimidazolium chloride (dimensionless)
[BMIM]DBP 1-butyl-3-methylimidazolium dibutylphosphate (dimensionless)
[BMIM]$MeSO_4$ 1-butyl-3-methylimidazolium methylsulfate (dimensionless)
[BMIM]PF_6 1-butyl-3-methylimidazolium hexafluorophosphate (dimensionless)
[BMIM]Tf_2N 1-butyl-3-methylimidazolium bis(trifluoromethylsulfonyl)imide (dimensionless)
[BMIM]TfO 1-butyl-3-methylimidazolium trifluoromethanesulfonate (dimensionless)
[C_{10}MIM]Br 1-decyl-3-methylimidazolium bromide (dimensionless)
[C_{10}MIM]Cl 1-decyl-3-methylimidazolium chloride (dimensionless)
[C_nMIM]BF_4 1-alkyl-3-methylimidazolium tetrafluoroborate, n=1, 2,... (dimensionless)
[C_nMIM]Cl 1-alkyl-3-methylimidazolium chloride, n=1, 2,... (dimensionless)
[C_nMIM]DMP 1-alkyl-3-methylimidazolium dimethylphosphate, n=1, 2,... (dimensionless)
[C_nMIM]$EtSO_4$ 1-alkyl-3-methylimidazolium ethylsulfate, n=1, 2,... (dimensionless)
[C_nMIM]$MeSO_4$ 1-alkyl-3-methylimidazolium methylsulfate, n=1, 2,... (dimensionless)
[C_nMIM]PF_6 1-alkyl-3-methylimidazolium hexafluorophosphate, n=1, 2,... (dimensionless)
[C_nMIM]Tf_2N 1-alkyl-3-methylimidazolium bis(trifluoromethylsulfonyl)imide, n=1, 2,... (dimensionless)
[C_nMIM]TfO 1-alkyl-3-methylimidazolium trifluoromethanesul fonate, n=1, 2,... (dimensionless)
[DMEA]Ac N,N-dimethylethanolammonium acetate (dimensionless)
[DMIM]BF_4 1-methyl-3-methylimidazolium tetrafluoroborate (dimensionless)
[DMIM]Cl 1,3-dimethylimidazolium chloride (dimensionless)
[DMIM]DMP 1,3-dimethylimidazolium dimethylphosphate (dimensionless)
[EEIM]DEP 1-ethyl-3-ethyl-imidazolium diethylphosphate (dimensionless)
[EMIM]BEI 1-ethyl-3-methylimidazolium bis(pentafluoroethyl sulfonyl)imide (dimensionless)
[EMIM]BF_4 1-ethyl-3-methylimidazolium tetrafluoroborate (dimensionless)
[EMIM]Br 1-ethyl-3-methylimidazolium bromide (dimensionless)
[EMIM]Cl1-ethyl-3-methylimidazolium chloride (dimensionless)
[EMIM]DEP 1-ethyl-3-methylimidazolium diethylphosphate (dimensionless)
[EMIM]DMP 1-ethyl-3-methylimidazolium dimethylphosphate (dimensionless)
[EMIM]$EtSO_4$ 1-ethyl-3-methylimidazolium ethylsulfate (dimensionless)
[EMIM]Tf_2N 1-ethyl-3-methylimidazolium bis(trifluoromethylsulfonyl)imide (dimensionless)
[EMIM]TfO 1-ethyl-3-methylimidazolium trifluoromethanesulfonate (dimensionless)
[HMIM]BF_4 1-hexyl-3-methylimidazolium tetrafluoroborate (dimensionless)
[HMIM]Cl 1-hexyl-3-methylimidazolium chloride (dimensionless)

$[HMIM]PF_6$ 1-hexyl-3-methylimidazolium hexafluorophosphate (dimensionless)
$[HMIM]Tf_2N$ 1-hexyl-3-methylimidazolium bis(trifluoromethylsulfonyl)imide (dimensionless)
[HMIM]TfO 1-hexyl-3-methylimidazolium trifluoromethanesulfonate (dimensionless)
$[HydeMIM]BF_4$ 1-(2-hydroxyethyl)-3-methylimidazolium tetra fluoroborate (dimensionless)
$[N_{111(2OH)}]Cl$ choline chloride (dimensionless)
[P4444]TMPP tetrabutylphosphonium bis(2,4,4-trimethylpentyl) phosphinate (dimensionless)
[P8111]TMPP trimethyloctylphosphonium bis(2,4,4-trimethyl pentyl)phosphinate (dimensionless)

Greek Letters

γ_i activity coefficient of species i (dimensionless), i=1, 2, 1 presents refrigerant, 2 presents absorbant
$\Delta_{eva}h_{TG}$ latent heat of evaporation of the refrigerant at T_G (kJ kg^{-1})
$\Delta_{mix}h$ mixing enthalpy of the system (kJ kg^{-1})
η_E system exergy efficiency (dimensionless)
ρ density (g cm^{-3})
ψ_1 absorption potential of the refrigerant species (dimensionless)

Superscripts

C combinatorial term (dimensionless)
R residual term (dimensionless)
RL Raoult's law (dimensionless)
∞ infinite dilution state (dimensionless)

Subscripts

A absorber (dimensionless)
C condenser (dimensionless)
E evaporator (dimensionless)
G generator (dimensionless)
max maximum value (dimensionless)
p poor solution (dimensionless)
r rich solution (dimensionless)

Acknowledgement

This work is supported by the National Natural Science Foundation of China (51276010), the National Basic Research Program of China (2010CB227304), and the China Postdoctoral Science Foundation funded project (No. 2013M540844).

References

[1] Ziegler F. State of the art in sorption heat pumping and cooling technologies. Int J Refrig 2002;25:450–9.
[2] Erickson DC, Anand G, Kyung I. Heat-activated dual-function absorption cycle. ASHRAE Trans 2004;110:515–24.
[3] Kim DS, Ferreira CA. Solar refrigeration options – a state of the art review. Int J Refrig 2008;31:3–15.
[4] Swarnkar SK, Venkatarathnam G, Ayou DS, Bruno JC, Coronas A. A review on absorption heat pumps and chillers using ionic liquids as absorbents. In: International workshop on ionic liquids–seeds for new engineering applications. Lisbon; 2012.
[5] Zheng DX, Chen B, Qi Y, Jin HG. Thermodynamic analysis of a novel absorption power/cooling combined-cycle. Appl Energy 2006;83:311–23.
[6] Deng J, Wang RZ, Han GY. A review of thermally activated cooling technologies for combined cooling, heating and power systems. Prog Energy Combust Sci 2011;37:172–203.
[7] Ma SL, Wang JF, Yan ZQ, Dai YP, Lu BH. Thermodynamic analysis of a new combined cooling, heat and power system driven by solid oxide fuel cell based on ammonia–water mixture. J Power Sources 2011;196:8463–71.
[8] Fukuta M, Yanagisawa T, Iwata H, Tada K. Performance of compression/absorption hybrid refrigeration cycle with propane/mineral oil combination. Int J Refrig 2002;25:907–15.
[9] Jelinek M, Levy A, Borde I. Performance of a triple-pressure level absorption/compression cycle. Appl Therm Eng 2012;42:2–5.
[10] Li Y, Saha TK, Krause O, Cao YJ. An inductively active filtering method for power quality improvement of distribution networks with nonlinear loads. IEEE Trans Power Deliv 2013;28:2465–73.
[11] Li G, Hwang Y, Radermacher R, Chun H. Review of cold storage materials for subzero applications. Energy 2013;51:1–17.
[12] Wang R, Yu X, Ge T, Li T. The present and future of residential refrigeration, power generation and energy storage. Appl Therm Eng 2013;53:256–70.
[13] Li G. Review of thermal energy storage technologies and experimental investigation of adsorption thermal energy storage for residential application (thesis). University of Maryland at College Park: United States; 2013.
[14] Li G, Hwang Y, Radermacher R. Review of cold storage materials for air conditioning application. Int J Refrig 2012;35:2053–77.
[15] Li G, Qian S, Lee H, Hwang Y, Radermacher R. Experimental investigation of energy and exergy performance of short term adsorption heat storage for residential application. Energy 2014;65:675–91.
[16] Wongsuwang W, Kumar S, Neveu P, Meunier F. A review of chemical heat pump technology and applications. Appl Therm Eng 2001;21:1489–519.
[17] Wu DW, Wang RZ. Combined cooling heating and power, a review progress in combustion. Energy Sci 2006;3:459–95.
[18] Petchers N. Combined heating, cooling & power handbook: technologies & applications an integrated approach to energy resource optimization. 2nd ed. Lilburn, GA: The Fairmont Press; 2012.
[19] Sun J, Fu L, Zhang SG. Performance calculation of single effect absorption heat pump using $LiBr+LiNO_3+H_2O$ as working fluid. Appl Therm Eng 2010;30:2680–4.
[20] De Lucas A, Donate M, Rodríguez JF. Applying surfactants to improve the absorption capacity of mixtures of lithium bromide and formates in absorption refrigeration coolers. Int J Refrig 2008;31:1073–80.
[21] Wu Y, Chen Y, Wu T. Experimental researches on characteristics of vapor–liquid equilibrium of NH_3–H_2O–LiBr system. Int J Refrig 2006;29:328–35.
[22] Ramesh Kumar A, Udayakumar M. Comparison of the performances of NH_3–H_2O, NH_3–$LiNO_3$ and NH_3–NaSCN GAX and GAX absorption–compression (GAXAC) cooler. In: Proceedings of the international sorption heat pump conference. Seoul; 2008.
[23] Yokozeki A, Shiflett MB. Ammonia solubilities in room-temperature ionic liquids. Ind Eng Chem Res 2007;46:1605–10.
[24] Herraiz J, Olive F, Zhu S, Shen S, Coronas A. Thermophysical properties of 2,2,2-trifluoroethanol+tetraethylene glycol dimethyl ether. J Chem Eng Data 1999;44:750–6.
[25] Coronas A, Valles M, Chaudhari SK, Patil KR. Absorption heat pump with the TFE-TEGDME and TFE–H_2O–TEGDME systems. Appl Therm Eng 1996;16:335–45.
[26] Xu S, Liu Y, Zhang L. Performance research of self-regenerated absorption heat transformer cycle using TFE-NMP as working fluids. Int J Refrig 2001;24:510–8.
[27] Nowaczyk U, Steimle F. Thermophysical properties of new working fluid systems for absorption processes. Int J Refrig 1992;15:10–5.
[28] Lee JW, Kim KS, Lee H. Vapor pressures and vapor–liquid equilibria of the 2,2,2-trifluoroethanol+quinoline system. J Chem Eng Data 2003;48:314–6.
[29] Kim KS, Lee JW, Kim JS, Lee H. Heat capacity measurement and cycle simulation of the trifluoroethanol (TFE)+quinoline mixture as a new organic working fluid used in absorption heat pump. Korean J Chem Eng 2003;20:762–7.
[30] Sand J.R., Fischer S.K., Baxter V.D. Energy and global warming impacts of HFC refrigerants and emerging technologies. Alternative Fluorocarbons Environmental Acceptability Study (AFEAS) and US; 1997.
[31] Kumar S, Prévost M, Bugarel R. Experimental studies of a three-pressure absorption refrigeration cycle. Int J Refrig 1993;16:31–9.
[32] Calm JM. The next generation of refrigerants—historical review, considerations, and outlook. Int J Refrig 2008;31:1123–33.
[33] Seddon KR. Ionic liquids for clean technology. J Chem Technol Biotechnol 1997;68:351–6.
[34] Wilkes JS, Zaworotko MJ. Air and water stable 1-ethyl-3-methylimidazolium based ionic liquids. J Chem Soc Chem Commun 1992;13:965–7.
[35] Bonhote P, Dias AP, Armand M. Hydrophobic, highly conductive ambient temperature molten salts. Inorg Chem 1996;35:1168–78.
[36] Jaiton D, Consorti Crestina S. Room temperature molten salts: neoteric green solvents for chemical reactions and process. J Braz Chem Soc 2000;11:337.
[37] Wasserscheid P, Waffenschmidt H. Ionic liquids in regioselective platinum-catalysed hydroformylation. J Mol Catal A: Chem 2000;164:61–7.
[38] Thomas W. Room temperature ionic liquids solvents for synthesis and catalysis. Chem Rev 1999;99:2071–83.
[39] Chiappe C, Neri L, Pieraccini D. Application of hydrophilic ionic liquids as co-solvents in chloroperoxidase catalyzed oxidations. Tetrahedron Lett 2006;47:5089–93.

[40] Violina A, Cocalia JD, Holbrey KE. Separations of metal ions using ionic liquids: the challenges of multiple mechanisms. Tsinghua Sci Technol 2006;11:188–93.
[41] Barhdadi R, Courtinard C, Nédélec JY, Troupel M. Room-temperature ionic liquids as new solvents for organic electrosynthesis. The first examples of direct or nickel-catalysed electroreductive coupling involving organic halides. Chem Commun 2003;12:1434–5.
[42] Kim KS, Shin BK, Lee H, Ziegler F. Refractive index and heat capacity of 1-butyl-3-methylimidazolium bromide and 1-butyl-3-methylimidazolium tetrafluoroborate, and vapor pressure of binary systems for 1-butyl-3-methylimidazolium bromide + trifluoroethanol and 1-butyl-3-methylimidazolium tetrafluoroborate + trifluoroethanol. Fluid Phase Equilib 2004;218:215–20.
[43] Kim KS, Park SY, Choi S, Lee H. Vapor pressures of the 1-butyl-3-methylimidazolium bromide + water, 1-butyl-3-methylimidazolium tetrafluoroborate + water, and 1-(2-hydroxyethyl)-3-methylimidazolium tetrafluoroborate + water systems. J Chem Eng Data 2004;49:1550–3.
[44] Shiflett MB, Yokozeki A. Solubilities and diffusivities of carbon dioxide in ionic liquids: [Bmim][PF_6] and [Bmim][BF_4]. Ind Eng Chem Res 2004;44:4453–64.
[45] Sen M, Paolucci S. Using carbon dioxide and ionic liquids for absorption refrigeration. In: Proceedings of the 7th IIR Gustav Lorentzen conference on natural working fluids; 2006.
[46] Shiflett MB, Yokozeki A. Absorption cycle using ionic liquids as working fluids. US2006/0197053 A1; 2006.
[47] Shiflett MB, Yokozeki A. Absorption cycle utilizing ionic liquid as working fluid. In: The 22nd international congress of refrigeration; 2007.
[48] Shiflett MB, Yokozeki A. Absorption cycle utilizing ionic liquids and water as working fluids. US2007/0144186 A1; 2007.
[49] Yokozeki A, Shiflett MB. Water solubility in ionic liquids and application to absorption cycles. Ind Eng Chem Res 2010;49:9496–503.
[50] Yokozeki A, Shiflett MB. Vapor–liquid equilibria of ammonia + ionic liquid mixtures. Appl Energy 2007;84:1258–73.
[51] Shiflett MB, Yokozeki A. Solubility of CO_2 in room-temperature ionic liquid [Hmim][Tf_2N]. J Phys Chem B 2007;111:2070–4.
[52] Yokozeki A, Shiflett MB. Global phase behaviors of trifluoromethane in room-temperature ionic liquid [Bmim][PF_6]. AIChE J 2006;52:3952–7.
[53] Shiflett MB, Harmer MA, Junk CP, Yokozeki A. Solubility and diffusivity of difluoromethane in room-temperature ionic liquids. J Chem Eng Data 2006;51:483–95.
[54] Shiflett MB, Yokozeki A. Solubility and diffusivity of hydrofluorocarbons in room-temperature ionic liquids. AIChE J 2006;52:1205–19.
[55] Shiflett MB, Yokozeki A. Separation of difluoromethane and pentafluoroethane by extractive distillation using ionic liquid. Chem Today 2006;24:28–30.
[56] Shiflett MB, Yokozeki A. Vapor–liquid–liquid equilibria of pentafluoroethane and ionic liquid [Bmim][PF_6] mixtures studied with the volumetric method. J Phys Chem B 2006;110:14436–43.
[57] Shiflett MB, Yokozeki A. Vapor–liquid–liquid equilibria of hydrofluorocarbons + 1-butyl-3- methylimidazolium hexafluorophosphate. J Chem Eng Data 2006;51:1931–9.
[58] Shiflett MB, Yokozeki A. Gaseous absorption of fluoromethane, fluoroethane, 1,1,2,2-Tetrafluoroethane in 1-butyl-3-methylidazolium hexafluorophosphate. Ind Eng Chem Res 2006;45:6375–82.
[59] Shiflett MB, Yokozeki A. Solubility differences of halocarbon isomers in ionic liquid [emim][Tf_2N]. J Chem Eng Data 2007;52:2007–15.
[60] Shiflett MB, Yokozeki A. Liquid liquid equilibria in binary mixtures containing fluorinated benzenes and ionic liquid 1-ethyl-3-methylimidazolium bis (trifluoromethylsulfonyl)imide. J Chem Eng Data 2008;53:2683–91.
[61] Shiflett MB, Yokozeki A. Binary vapor–liquid and vapor–liquid–liquid equilibria of hydrofluorocarbons (HFC-125 and HFC-143a) and hydrofluoroethers (HFE-125 and HFE-143a) with ionic liquid [emim][Tf2N]. J Chem Eng Data 2008;53:492–7.
[62] Shiflett MB, Harmer MA, Junk CP, Yokozeki A. Solubility and diffusivity of 1,1,1,2-tetrafluoroethane in room-temperature ionic liquids. Fluid Ph Equilib 2006;242:220–32.
[63] Martín A, Bermejo MD. Thermodynamic analysis of absorption refrigeration cycles using ionic liquid + supercritical CO_2 pairs. J Supercrit Fluids 2010;55:852–9.
[64] Kim S, Kim YJ, Joshi YK, Fedorov AG, Kohl PA. Absorption heat pump/refrigeration system utilizing ionic liquid and hydrofluorocarbon refrigerants. J Electron Packag, Trans ASME 2012:134 (no. 031009).
[65] Kim YJ, Kim S, Joshi YK, Fedorov AG, Kohl PA. Thermodynamic analysis of an absorption refrigeration system with ionic-liquid/refrigerant mixture as a working fluid. Energy 2012;44:1005–16.
[66] Liang SQ, Zhao J, Wang L, Huai XL. Absorption refrigeration cycle utilizing a new working pair of ionic liquid type. Kung Cheng Je Wu Li Hsueh Pao/J Eng Thermophys 2010;31:1627–30.
[67] Zhao J, Liang SQ, Chen J, Wang L, Huai XL. Vapor–liquid equilibrium for high concentration solution of 1,3-dimethylimidazolium dimethyl phosphate–methanol. Huaxue Gongcheng/Chem Eng (China) 2010;38:52–6.
[68] Zhang XD, Hu DP. Performance simulation of the absorption chiller using water and ionic liquid 1-ethyl-3-methylimidazolium dimethylphosphate as the working pair. Appl Therm Eng 2011;31:3316–21.
[69] Zhang X, Hu D, Zhao Z. Thermodynamic performance of absorption heat transformer using a new working pair: water + ionic liquid 1,3-dimethylimidazolium dimethylphosphate. Adv Mater Res 2012;512–515:1258–62.
[70] Zhang XD, Hu DP. Performance analysis of the single-stage absorption heat transformer using a new working pair composed of ionic liquid and water. Appl Therm Eng 2012;37:129–35.
[71] Dong L, Zheng D, Li J, Nie N, Wu X. Suitability prediction and affinity regularity assessment of H_2O + imidazolium ionic liquid working pairs of absorption cycle by excess property criteria and UNIFAC model. Fluid Phase Equilib 2013;348:1–8.
[72] Dong L, Zheng D, Nie N, Li Y. Performance prediction of absorption refrigeration cycle based on the measurements of vapor pressure and heat capacity of H_2O + [DMIM]DMP system. Appl Energy 2012;98:326–32.
[73] Dong L, Zheng D, Sun G, Wu X. Vapor–liquid equilibrium measurement of difluorometha + [Emim]TfO, difluoromethane + [Bmim]TfO, difluoroethane + [Emim]TfO and difluoroethane + [Bmim]TfO. J Chem Eng Data 2011;56:3663–8.
[74] Dong L, Zheng D, Wei Z, Wu X. Synthesis of 1,3-dimethylimidazolium chloride and volumetric property investigations of its aqueous solution. Int J Thermophys 2009;30:1480–90.
[75] Dong L, Zheng DX, Wu XH. Working pair selection of compression and absorption hybrid cycles through predicting the activity coefficients of hydrofluorocarbon + ionic liquid systems by UNIFAC model. Ind Eng Chem Res 2012;51:4741–7.
[76] Li J, Zheng D, Fang L, Wu X, Dong L. Vapor pressure measurement of the ternary systems H_2O + LiBr + [Dmim]Cl, H_2O + LiBr + [Dmim]BF_4, H_2O + LiCl + [Dmim]Cl and H_2O + LiCl + [Dmim]BF_4. J Chem Eng Data 2011;56:97–101.
[77] Nie N, Zheng D, Dong L, Li Y. Thermodynamic properties of water + 1-(2-hydroxylethyl)-3-methylimidazolium chloride system. J Chem Eng Data 2012;57:3598–603.
[78] Sun GM, Zheng DX, Huang WJ, Dong L. The measurement of ammonia solubility in ionic liquid [Dmim]DMP. J Beijing Univ Chem Technol (Nat Sci) 2012;39:17–21 (in Chinese).
[79] Sun G, Huang W, Zheng D, Dong L, Wu X. Vapor–liquid equilibrium prediction of ammonia-ionic liquid working pairs of absorption cycle using UNIFAC model. Chin J Chem Eng 2014;22:72–8.
[80] Wang JZ, Zheng DX, Fan LH, Dong L. Vapor pressure measurements for water + 1,3-dimethylimidazolium chloride system and 2,2,2-trifluoroethanol + 1-ethyl-3-methylimidazolium tetrafluoroborate system. J Chem Eng Data 2010;55:2128–32.
[81] Wang JZ, Zheng DX. Performance analysis of absorption cooling cycle utilizing TFE-[BMIm]Br as working fluid. Kung Cheng Je Wu Li Hsueh Pao/J Eng Thermophys 2008;29:1813–6.
[82] Wu X, Li J, Fan L, Zheng D, Dong L. Vapor pressure measurement of water + 1,3-dimethylimidazolium tetrafluoroborate system. Chin J Chem Eng 2011;19:473–7.
[83] Wu X, Zheng D. A new approach for appropriate absorbent selection with excess Gibbs function. In: Proceedings of the 18th European conference on thermophysical properties, Paper No. 413; 2008.
[84] Smith JM, Van Ness HC, Abbott MM. Introduction to chemical engineering thermodynamics. 6th ed. New York: McGraw-Hill; 2002.
[85] Sandler SI. Chemical and engineering thermodynamics. 3rd ed. New York: John Wiley & Sons, Inc; 1999.
[86] Iedema PD. Mixtures for the absorption heat pump. Int J Refrig 1982;5:262–73.
[87] Morrissey AJ, O'Donnell JP. Endothermic solutions and their application in absorption heat pumps. Chem Eng Res Des 1986;64:404–6.
[88] Shi W, Maginn EJ. Molecular simulation of ammonia absorption in the ionic liquid 1-ethyl-3-methylimidazolium bis(trifluoromethylsulfonyl)imide ([emim][Tf_2N]). AIChE J 2009;55:2414–21.
[89] Greenwood NN, Earnshaw A. Chemistry of the elements. 2nd ed. Oxford: Butterworth-Heinemann Ltd; 1997.
[90] Pauling L. The origin and nature of the electronegativity scale. J Chem Educ 1988;65:375.
[91] Klimavicius V, Gdaniec Z, Kausteklis J, Aleksa V, Aidas K, Balevicius V. NMR and Raman spectroscopy monitoring of proton/deuteron exchange in aqueous solutions of ionic liquids forming hydrogen bond: a role of anions, self-aggregation, and mesophase formation. J Phys Chem B 2013;117:10211–20.
[92] D'Angelo P, Zitolo A, Aquilanti G, Migliorati V. Using a combined theoretical and experimental approach to understand the structure and dynamics of imidazolium-based ionic liquids/water mixtures. 2. EXAFS spectroscopy. J Phys Chem B 2013;117:12516–24.
[93] Cammarata L, Kazarian SG, Salter PA, Welton T. Molecular states of water in room temperature ionic liquids. Phys Chem Chem Phys 2001;3:5192–200.
[94] Fredenslund A, Jones RL, Prausnitz JM. Group-contribution estimation of activity coefficients in nonideal liquid mixtures. AIChE J 1975;21:1086–99.
[95] Stoppa A, Hunger J, Buchner R. Conductivities of binary mixtures of ionic liquids with polar solvents. J Chem Eng Data 2009;54:472–9.
[96] Ren W, Scurto AM. Phase equilibria of imidazolium ionic liquids and the refrigerant gas, 1,1,1,2-tetrafluoroethane (R-134a). Fluid Ph Equilib 2009;286:1–7.
[97] Wittig R, Lohmann J, Gmehling J. Vapor–liquid equilibria by UNIFAC group contribution. 6. Revision and extension. Ind Eng Chem Res 2003;42:183–8.
[98] Kim YS, Choi WY, Jang JH. Solubility measurement and prediction of carbon dioxide in ionic liquids. Fluid Ph Equilib 2005;228–229:439–45.
[99] Lei ZG, Zhang JG, Li QS, Chen BH. UNIFAC model for ionic liquids. Ind Eng Chem Res 2009;48:2697–704.
[100] Kleiber M. An extension to the UNIFAC group assignment for prediction of vapor-liquid equilibria of mixtures containing refrigerants. Fluid Ph Equilib 1995;107:161–88.
[101] Prausnitz JM, Lichenthaler RN, De Azevedo EG. Molecular thermodynamics of fluid-phase equilibria. 3rd ed. Englewood Cliffs: Prentice Hall PTR; 1999.

[102] Narodoslawsky M, Otter G, Moser F. Thermodynamic criteria for optimal absorption heat pump media. Heat Recovery Syst CHP 1988;8:221–33.
[103] Narodoslawsky M, Otter G, Moser F. New working pairs for medium and high temperature industrial absorption heat pumps. Heat Recovery Syst CHP 1988;8:459–68.
[104] Calvar N, Gonzalez B, Gomez E, Domınguez A. Vapor–liquid equilibria for the ternary system ethanol+water+1-butyl-3-methylimidazolium chloride and the corresponding binary systems at 101.3 kPa. J Chem Eng Data 2006;51:2178–81.
[105] Calvar N, Gonzalez B, Gomez E, Dominguez A. Vapor liquid equilibria for the ternary system ethanol+water+1-ethyl-3-methylimidazolium ethylsulfate and the corresponding binary systems containing the ionic liquid at 101.3 kPa. J Chem Eng Data 2008;53:820–5.
[106] Calvar N, Gonzalez B, Gomez E, Dominguez A. Vapor–liquid equilibria for the ternary system ethanol+water+1-butyl-3-methylimidazolium methylsulfate and the corresponding binary systems at 101.3 kPa. J Chem Eng Data 2009;54:1004–8.
[107] Doker M, Gmehling J. Measurement and prediction of vapor–liquid equilibria of ternary systems containing ionic liquids. Fluid Ph Equilib 2005;227:255–66.
[108] Guo KH, Bi Y, Sun L, Su H, Huangpu LX. Experiment and correlation of vapor–liquid equilibrium of aqueous solutions of hydrophilic ionic liquids: 1-ethyl-3-methylimidazolium acetate and 1-hexyl-3-methylimidazolium chloride. J Chem Eng Data 2012;57:2243–51.
[109] He ZB, Zhao ZC, Zhang XD, Feng H. Thermodynamic properties of new heat pump working pairs: 1,3-dimethylimidazolium dimethylphosphate and water, ethanol and methanol. Fluid Ph Equilib 2010;298:83–91.
[110] Jiang XC, Wang JF, Li CX, Wang LM, Wang ZH. Vapour pressure measurement for binary and ternary systems containing water methanol ethanol and an ionic liquid 1-ethyl-3-ethylimidazolium diethylphosphate. J Chem Thermodyn 2007;39:841–6.
[111] Jork C, Seiler M, Beste YA, Arlt W. Influence of ionic liquids on the phase behavior of aqueous azeotropic systems. J Chem Eng Data 2004;49:852–7.
[112] Kato R, Gmehling J. Measurement and correlation of vapor liquid equilibria of binary systems containing the ionic liquids [EMIM][$(CF_3SO_2)_2N$], [BMIM][$(CF_3SO_2)_2N$], [MMIM][$(CH_3)_2PO_4$] and oxygenated organic compounds respectively water. Fluid Ph Equilib 2005;231:38–43.
[113] Ren J, Zhao ZC, Zhang XD. Vapor pressures, excess enthalpies, and specific heat capacities of the binary working pairs containing the ionic liquid 1-ethyl-3-methylimidazolium dimethylphosphate. J Chem Thermodyn 2011;43:576–83.
[114] Simoni LD, Ficke LE, Lambert CA. Measurement and prediction of vapor–liquid equilibrium of aqueous 1-ethyl-3-methylimidazolium-based ionic liquid systems. Ind Eng Chem Res 2010;49:3893–901.
[115] Sumartschenkowa IA, Verevkin SP, Vasiltsova TV. Experimental study of thermodynamic properties of mixtures containing ionic liquid 1-ethyl-3-methylimidazolium ethyl sulfate using gas–liquid chromatography and transpiration method. J Chem Eng Data 2006;51:2138–44.
[116] Wang JF, Li CX, Wang ZH. Vapor pressure measurement for water, methanol, ethanol and their binary mixtures in the presence of an ionic liquid 1-ethyl-3-methylimidazolium dimethylphosphate. Fluid Ph Equilib 2007;255:186–92.
[117] Wang JF, Wang DG, Li ZB. Vapor pressure measurement and correlation or prediction for water, 1-propanol, 2-propanol, and their binary mixtures with [MMIM][DMP] ionic liquid. J Chem Eng Data 2010;55:4872–7.
[118] Zhao J, Jiang XC, Li CX, Wang ZH. Vapor pressure measurement for binary and ternary systems containing a phosphoric ionic liquid. Fluid Ph Equilib 2006;247:190–8.
[119] Zuo GL, Zhao ZC, Yan SH, Zhang XD. Thermodynamic properties of a new working pair: 1-ethyl-3-methylimidazolium ethylsulfate and water. Chem Eng J 2010;156:613–7.
[120] Carvalho PJ, Khan I, Morais A, Granjo JFO, Oliveira NMC, Santos LM NBF Coutinho JAP. A new microebulliometer for the measurement of the vapor–liquid equilibrium of ionic liquid systems. Fluid Ph Equilib 2013;354:156–65.
[121] Królikowska M, Karpińska M, Zawadzki M. Phase equilibria study of (ionic liquid+water) binary mixtures. Fluid Ph Equilib 2013;354:66–74.
[122] Ficke LE, Rodriguez H, Brennecke JF. Heat capacities and excess enthalpies of 1-ethyl-3-methylimidazolium-based ionic liquids and water. J Chem Eng Data 2008;53:2112–9.
[123] Garcia-Miaja G, Troncoso J, Romani L. Excess enthalpy, density, and heat capacity for binary systems of alkylimidazolium-based ionic liquids+water. J Chem Thermodyn 2009;41:161–6.
[124] Lin PY, Soriano AN, Leron RB. Measurements and correlations of electrolytic conductivity and molar heat capacity for the aqueous ionic liquid systems containing [Emim][$EtSO_4$] or [Emim][CF_3SO_3]. Exp Therm Fluid Sci 2011;35:1107–12.
[125] Lin PY, Soriano AN, Caparanga AR. Molar heat capacity and electrolytic conductivity of aqueous solutions of [Bmim][$MeSO_4$] and [Bmim][triflate]. Thermochim Acta 2009;496:105–9.
[126] Rebelo LPN, Najdanovic-Visak V, Visak ZP. A detailed thermodynamic analysis of [C_4mim][BF_4]+water as a case study to model ionic liquid aqueous solutions. Greem Chem 2004;6:369–81.
[127] Zhang SJ, Li X, Chen HP, Wang JF, Zhang JM, Zhang ML. Determination of physical properties for the binary system of 1-ethyl-3-methylimidazolium tetrafluoroborate+H_2O. J Chem Eng Data 2004;49:760–4.
[128] Zhou Q, Wang LS, Chen HP. Densities and viscosities of 1-butyl-3-methylimidazolium tetrafluoroborate+H_2O binary mixtures from (303.15 to 353.15) K. J Chem Eng Data 2006;51:905–8.
[129] Lu XM, Xu WG, Gui JS. Volumetric properties of room temperature ionic liquid 1. The system of {1-methyl-3-ethylimidazolium ethyl sulfate+water} at temperature in the range (278.15 to 333.15) K. J Chem Thermodyn 2005;37:13–9.
[130] Yang JZ, Lu XM, Gui JS, Xu WG, Li HW. Volumetric properties of room temperature ionic liquid 2. The concentrated aqueous solutions of {1-methyl-3-ethylimidazolium ethyl sulfate+water} in a temperature range of 278.2 K to 338.2 K. J Chem Thermodyn 2005;37:1250–5.
[131] Carvalho PJ, Regueira T, Santos LM. Effect of water on the viscosities and densities of 1-butyl-3-methylimidazolium dicyanamide and 1-butyl-3-methylimidazolium tricyanomethane at atmospheric pressure. J Chem Eng Data 2010;55:645–52.
[132] Gaillon L, Sirieix-Plenet J, Letellier P. Volumetric study of binary solvent mixtures constituted by amphiphilic ionic liquids at room temperature (1-alkyl-3-methylimidazolium bromide) and water. J Solut Chem 2004;33: 1333–47.
[133] Gomez E, Gonzalez B, Dominguez A. Dynamic viscosities of a series of 1-alkyl-3-methylimidazolium chloride ionic liquids and their binary mixtures with water at several temperatures. J Chem Eng Data 2006;51:696–701.
[134] Gomez E, Gonzalez B, Calvar N. Physical properties of pure 1-ethyl-3-methylimidazolium ethylsulfate and its binary mixtures with ethanol and water at several temperatures. J Chem Eng Data 2006;51:2096–102.
[135] Gonzalez B, Calvar N, Gomez E. Physical properties of the ternary system (ethanol+water+1-butyl-3-methylimidazolium methylsulphate) and its binary mixtures at several temperatures. J Chem Thermodyn 2008;40:1274–81.
[136] Liu W, Cheng L, Zhang Y. The physical properties of aqueous solution of room-temperature ionic liquids based on imidazolium: database and evaluation. J Mol Liq 2008;140:68–72.
[137] Rilo E, Pico J, Garcia-Garabal S. Density and surface tension in binary mixtures of C_nMIM-BF_4 ionic liquids with water and ethanol. Fluid Ph Equilib 2009;285:83–9.
[138] Rodriguez H, Brennecke JF. Temperature and composition dependence of the density and viscosity of binary mixtures of water+ionic liquid. J Chem Eng Data 2006;51:2145–55.
[139] Vila J, Gines P, Rilo E. Great increase of the electrical conductivity of ionic liquids in aqueous solutions. Fluid Ph Equilib 2006;247:32–9.
[140] Li GH, Zhou Q, Zhang XQ. Solubilities of ammonia in basic imidazolium ionic liquids. Fluid Ph Equilib 2010;297:34–9.
[141] Chen W, Liang S, Guo Y, Gui X, Tang D. Investigation on vapor–liquid equilibria for binary systems of metal ion-containing ionic liquid [bmim]Zn_2Cl_5/NH_3 by experiment and modified UNIFAC model. Fluid Ph Equilib 2013;360:1–6.
[142] Kumełan J, Kamps AP, Tuma D, Yokozeki A, Shiflett MB, Maurer G. Solubility of tetrafluoromethane in the ionic liquid [hmim][Tf_2N]. J Phys Chem B 2008;112:3040–7.
[143] Shariati A, Peters CJ. High-pressure phase behavior of systems with ionic liquids: measurements and modeling of the binary system fluoroform+1-ethyl-3-methylimidazolium hexafluorophosphate. J Supercrit Fluids 2003;25:109–17.
[144] Lee B, Outcalt S. Solubilities of gases in the ionic liquid 1-n-butyl-3-methylimidazolium bis(trifluoromethylsulfonyl)imide. J Chem Eng Data 2006;51:892–7.
[145] Liu X, Ruiz E, Afzal W, Ferro VR, Palomar J, Prausnitz JM. High solubilities for methane, ethane, ethylene and propane in [P8111][TMPP]. Ind Eng Chem Res 2014;53:363–8.
[146] Liu X, Afzal W, Prausnitz JM. Solubilities of small hydrocarbons in tetrabutylphosphonium bis(2,4,4-trimethylpentyl) phosphinate and in 1-ethyl-3-methylimidazolium bis(trifluoromethylsulfonyl)imide. Ind Eng Chem Res 2013;52:14975–8.
[147] Nebig S, Gmehling J. Measurements of different thermodynamic properties of systems containing ionic liquids and correlation of these properties using modified UNIFAC (Dortmund). Fluid Ph Equilib 2010;294:206–12.
[148] Verevkin SP, Safarov J, Bich E, Hassel E, Heintz A. Thermodynamic properties of mixtures containing ionic liquids vapor pressures and activity coefficients of n-alcohols and benzene in binary mixtures with 1-methyl-3-butyl-imidazolium bis(trifluoromethyl-sulfonyl) imide. Fluid Ph Equilib 2005;236:222–8.
[149] Shen C, Li X, Lu Y, Li C. Effect of ionic liquid 1-methylimidazolium chloride on the vapour liquid equilibrium of water, methanol, ethanol, and {water+ethanol} mixture. J Chem Thermodyn 2011;43:1748–53.
[150] González EJ, Calvar N, Macedo EA. Osmotic coefficients and apparent molar volumes of 1-hexyl-3-methylimidazolium trifluoromethanesulfonate ionic liquid in alcohols. J Chem Thermodyn 2014;69:93–100.
[151] Zhang X, Hu D, Zhao Z. Measurement and prediction of vapor pressure for H_2O+CH_3OH/C_2H_5OH+[BMIM][DBP] ternary working fluids. Chin J Chem Eng 2013;21:886–93.
[152] Domanska U, Krolikowska M, Krolikowski M. Phase behaviour and physico-chemical properties of the binary systems {1-ethyl-3-methylimidazolium thiocyanate, or 1-ethyl-3-methylimidazolium tosylate+water, or+an alcohol}. Fluid Ph Equilib 2010;294:72–83.
[153] Gonzalez EJ, Alonso L, Dominguez A. Physical properties of binary mixtures of the ionic liquid 1-methyl-3-octylimidazolium chloride with methanol, ethanol, and 1-propanol at T=(298.15, 313.15, and 328.15) K and at P=0.1 MPa. J Chem Eng Data 2006;51:1446–52.
[154] Gong YH, Shen C, Lu YZ, Meng H, Li CX. Viscosity and density measurements for six binary mixtures of water (methanol or ethanol) with an ionic liquid

([BMIM][DMP] or [EMIM][DMP]) at atmospheric pressure in the temperature range of (293.15 to 333.15) K. J Chem Eng Data 2012;57:33–9.
[155] Rilo E, Varela LM, Cabeza O. Density and derived thermodynamic properties of 1-ethyl-3-methylimidazolium alkyl sulfate ionic liquid binary mixtures with water and with ethanol from 288 K to 318 K. J Chem Eng Data 2012;57:2136–42.
[156] Yao HW, Zhang SH, Wang JL, Zhou Q, Dong HF, Zhang XP. Densities and viscosities of the binary mixtures of 1-ethyl-3-methylimidazolium bis (trifluoromethylsulfonyl)imide with n-methyl-2-pyrrolidone or ethanol at $T=(293.15$ to $323.15)$ K. J Chem Eng Data 2012;57:875–81.
[157] Waliszewski D. Heat capacities of the mixtures of ionic liquids with methanol at temperatures from 283.15 K to 323.15 K. J Chem Thermodyn 2008;40: 203–7.
[158] Yokozeki A. Theoretical performances of various refrigerant-absorbent pairs in a vapor-absorption refrigeration cycle by the use of equations of state. Appl Energy 2005;80:383–99.
[159] Arivazhagan S, Murugesan SN, Saravanan R, Renganarayanan S. Simulation studies on R134a–DMAC based half effect absorption cold storage systems. Energy Convers Manag 2005;46:1703–13.